MSc Biomedical Engineering

Antibacterial Surfaces Bearing Silver, Copper and Zinc Nanoparticles on Additively Manufactured Titanium Implants

Master Thesis

Melissa Tierolf

Delft University of Technology

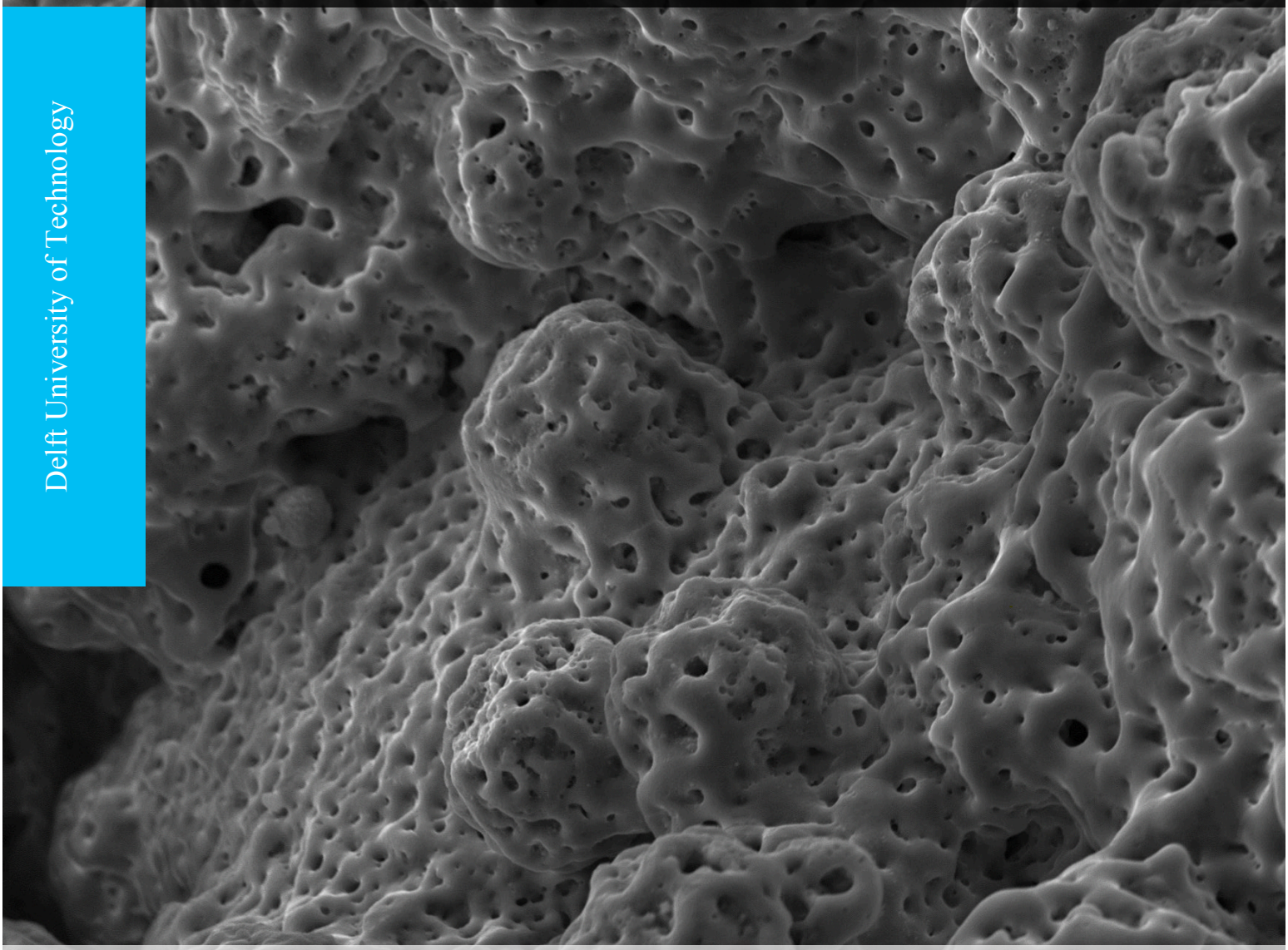

Supervisors: Dr. Ir. Lidy Fratila-Apachitei
Ir. Ingmar A.J. Van Hengel
Dr. Ad Fluit
Prof. Dr. Ir. Amir A. Zadpoor

TU Delft

Antibacterial Surfaces Bearing Silver, Copper and Zinc Nanoparticles on Additively Manufactured Titanium Implants

By
Melissa Tierolf
4502884

in partial fulfillment of the requirements for the degree of

Master of Science
in Biomedical Engineering

at the Delft University of Technology to be defended publicly on Thursday, March 7, 2019 at 16.00.

Supervisors: Dr. Ir. Lidy Fratila-Apachitei
Ir. Ingmar A.J. Van Hengel
Dr. Ad Fluit
Prof. Dr. Ir. Amir A. Zadpoor

Biomaterials and Tissue Biomechanics Specialization
Biomechanical Engineering Department
Faculty of Mechanical, Maritime, and Materials Engineering
Delft University of Technology

Abstract

BACKGROUND. Implant-associated infection (IAI) is a rising complication in bone-related medical treatments using metal implants. Preventive measures, such as implant surfaces with integrated antibacterial properties, are hence required. The emergence of antibiotic-resistant pathogens has led to a growing interest in inorganic nanoparticles as antibacterial agents. In addition, implants should simultaneously stimulate bone tissue regeneration and integration to improve implant longevity. Additive manufacturing (AM) of orthopedic implants has attracted interest as improved bone tissue regeneration and integration was demonstrated by AM porous implants. AM porous implants, however, are at enhanced risks of IAIs; these porous implants require integrated antibacterial properties. This study focused on a systematic comparison of the antibacterial properties of AM porous Ti6Al4V implant surfaces with silver nanoparticles (Ag NPs), copper nanoparticles (Cu NPs) and/or zinc nanoparticles (Zn NPs) against methicillin resistant *Staphylococcus aureus* (MRSA).

METHODS. Medical grade porous Ti6Al4V implants were additively manufactured using selective laser melting (SLM). Subsequently, the SLM Ti6Al4V implants were biofunctionalized by plasma electrolytic oxidation (PEO) using an electrolyte that consisted of Ca/P-based species and ratios of Ag NPs, Cu NPs and/or Zn NPs. Implants with 0, 25, 75 and 100% of Ag NPs, Cu NPs and/or Zn NPs were synthesized. After biofunctionalization, the surface morphology, structure and chemistry of the implants were investigated using scanning electron microscopy (SEM) and energy dispersive X-ray spectroscopy (EDS). The antibacterial properties of the implants against MRSA were studied *in vitro* as well as *ex vivo*. The leachable antibacterial activity was studied in an agar diffusion assay, the minimal inhibitory concentration (MIC) and minimal bactericidal concentration (MBC) of Ag^{+}, Cu^{2+} and Zn^{2+} ions was determined by a micro-dilution assay and the bactericidal activity of the implants was quantified by a colony-forming unit (CFU) count *in vitro* against surface-adherent and non-adherent MRSA. Furthermore, *ex vivo* antibacterial properties were determined using a femoral murine infection model mimicking the *in vivo* environment.

RESULTS. Biofunctionalization of the porous SLM Ti6Al4V implants by PEO resulted in a uniform and homogeneous micro-/nano-porous oxide layer that covered the entire surface of the implants. SEM and EDS analysis demonstrated the presence of Ag NPs, Cu NPs and Zn NPs in the TiO_2 surface layer. The agar diffusion assay demonstrated a strong leachable antibacterial activity for implants with Ag NPs and Cu NPs or Zn NPs, while no leachable antibacterial activity was observed for implants without Ag NPs. Antibacterial testing showed that Ag^{+}, Cu^{2+} and Zn^{2+} ions, as well the combinations of the ions, were growth inhibitory and bactericidal to MRSA. In addition, implants with $\geq$ 50% of Ag NPs and combinations of $\geq$ 75% of Ag NPs and Cu NPs or Zn NPs, fully eradicated surface-adherent and non-adherent MRSA within 24 h and prevented biofilm formation up to 24 h. Moreover, strong *ex vivo* bactericidal properties against MRSA were demonstrated for these implants within 24 h.

CONCLUSION. Biofunctionalized surfaces with Ag NPs and Cu NPs or Zn NPs on porous SLM Ti6Al4V implants showed strong *in vitro* and *ex vivo* antibacterial properties against MRSA. The implants with 50% of Ag NPs and combinations of 75% of Ag NPs and 25% of Cu NPs or Zn NPs are promising for further development, to prevent IAIs and improve the longevity of the implants in clinical applications.

Contents

1 Introduction

As a consequence of the aging of the world population and the increasing life expectancy, the incidence of musculoskeletal disorders and diseases such as bone fractures [1], osteoarthritis [2], osteoporosis [3] and bone metastases are expected to increase [4]. Bone-related medical treatments are therefore anticipated to surge, particularly the use of permanent metal implants [4]. Metal implants, however, are associated with complications, causing the implant to fail. Implant-associated infection (IAI) is a rising complication in bone-related medical treatments using metal implants [5].

The pathogenesis of early IAIs is determined by a bacterial invasion of the implantation site and subsequent bacterial adhesion on the implant surface [5-7]. Bacterial surface colonization is successively initiated and ultimately results in biofilm formation, which is crucial in the development of IAIs [7,8]. These biofilms offer extraordinary resistance to conventional antibiotics and the defense mechanism of the host. The susceptibility for IAIs is even further enhanced due to a compromised immune system of the host at the site of the implant [9]. As a result of the pathogenesis, IAIs are difficult to treat clinically and ultimately require surgery, which imposes significant social and economic burdens, estimated at $95,000 per case [10]. In addition, the probability of re-infection after 1-year treatment is 19%, since the biofilms promote the bacteria to migrate to the peri-implant area and the blood circulation [11].

Due to the difficulties in the treatment of IAIs and the associated burden on the patient and health care system, innovative cost-effective techniques that preserve implant surfaces from bacterial adhesion and inevitable biofilm formation have attracted interest, in particular surfaces with integrated active antibacterial properties [12-16]. The advantage of an implant surface with integrated active antibacterial properties is the ability to provide a controlled amount of antibacterial agents at the site of implantation. In addition, local delivery of antibacterial agents improves antibacterial efficacy and reduces the risk of systemic toxicity [17]. Numerous attempts were hence made to provide active antibacterial properties to the implant surface with different approaches, such as the incorporation of antibiotics in the surface of implants [18,19]. However, the emergence of antibiotic-resistant *Staphylococci* strains, which account for more than 50% of IAI cases, has made conventional antibiotics as methicillin ineffective [20].

By cause of the spread of antibiotic-resistant pathogens, research into inorganic nanoparticles as antibacterial agents, in particular silver nanoparticles (Ag NPs), copper nanoparticles (Cu NPs) and zinc nanoparticles (Zn NPs), has attracted interest [21]. The NPs have shown a wide spectrum of antibacterial properties against Gram-negative and Gram-positive bacteria [22-24], by means of multifaceted antibacterial mechanisms, among the release of ions, disruption of bacterial membranes and the generation of reactive oxygen species (ROS) [25,26]. Due to multifaceted antibacterial mechanisms, NPs have been shown to minimize antibacterial resistance potentials [27,28]. In addition to the antibacterial properties, Cu NPs and Zn NPs have demonstrated to stimulate bone tissue regeneration. Cu NPs and Zn NPs promoted osteogenesis by stimulation of the adhesion, proliferation and differentiation of the

mesenchymal stem cells (MSCs) [29,30]. In addition, Cu NPs and Zn NPs demonstrated to be less toxic on MSCs, as compared to Ag NPs [31-33]. The properties of the individual NPs are widely reported. However, recently synergy between silver (i.e. Ag NPs) and zinc (i.e Zn^{2+} ions) was demonstrated on antibacterial as well as on osteogenic properties [34,35]. In addition, a possible synergy was observed between silver and copper, as evidenced by a reduction in the minimum inhibitory concentration against Gram-negative and Gram-positive bacteria, including antibiotic-resistance pathogens [36,37]. This implies that cytotoxicity could be compensated through substitution of Ag NPs partly with Cu NPs or Zn NPs, without affecting the antibacterial properties.

Besides the prevention of IAIs, implants should simultaneously stimulate and support bone tissue regeneration and integration to improve implant longevity [38,39]. Multifunctional orthopedic biomaterials are hence required. At present, titanium (Ti) and its alloys are primarily used biomaterials in orthopedic fields, because of their intrinsic biocompatibility, prominent mechanical properties and anti-corrosion quality [40]. Titanium, however, is bio-inert and hence has poor bone-fixation ability [41]. Additive manufacturing (AM) of titanium implants has therefore gathered interest. AM techniques enable the production of highly porous biomaterials with mechanical properties closely related to the human bone [42]. Furthermore, geometric characteristics of porous biomaterials for instance the porosity [43], pore size [43,44] and pore shape [45] can be designed to stimulate the regeneration of bone tissue and implant integration [46]. AM techniques are hence able to fabricate highly complex, custom-designed topologies [47,48]. As a result, AM porous biomaterials could be suitable for the unmet clinical needs in cases of major bone defects [49], complex bone fractures [50] and prostheses for rescuing large limbs caused by metastases [51]. Unfortunately, morphological features of such biomaterials that stimulate tissue regeneration and integration, also promotes bacterial adhesion [52]. As a result, porous implants are at enhanced risks of IAIs. Hence, customized AM porous biomaterials require integrated antibacterial properties.

Antibacterial properties on AM porous implant surfaces have been synthesized by an electrochemical surface modification technique, plasma electrolytic oxidation (PEO). With the aid of PEO, surfaces with multiple functionalities could be obtained in one-step process. This is in contrast to many other conventional surface modification techniques, which comprises sequences of process steps [53,54]. PEO transforms a titanium surface into a ceramic-like, micro-/nano-porous and bioactive titanium oxide (TiO_2) layer, which improves the osseointegration [55-57], and simultaneously distributes tightly attached NPs homogeneously over the surface [58,59]. Porous AM titanium implants with Ag NPs synthesized by PEO, have demonstrated antibacterial properties *in vitro* as well as *ex vivo* against methicillin-resistant *Staphylococcus aureu*s (MRSA) [60]. To the author's best knowledge, the antibacterial properties of porous Ti-based surfaces with Ag NPs, Cu NPs and/or Zn NPs have not yet been investigated. Hence, the current study aimed to evaluate and systematically compare the antibacterial properties of AM porous Ti6Al4V implant surfaces with Ag NPs, Cu NPs and/or Zn NPs against MRSA.

2 Materials and Methods

2.1 Study design

An outline of the design of the current study is illustrated in Fig. 1.

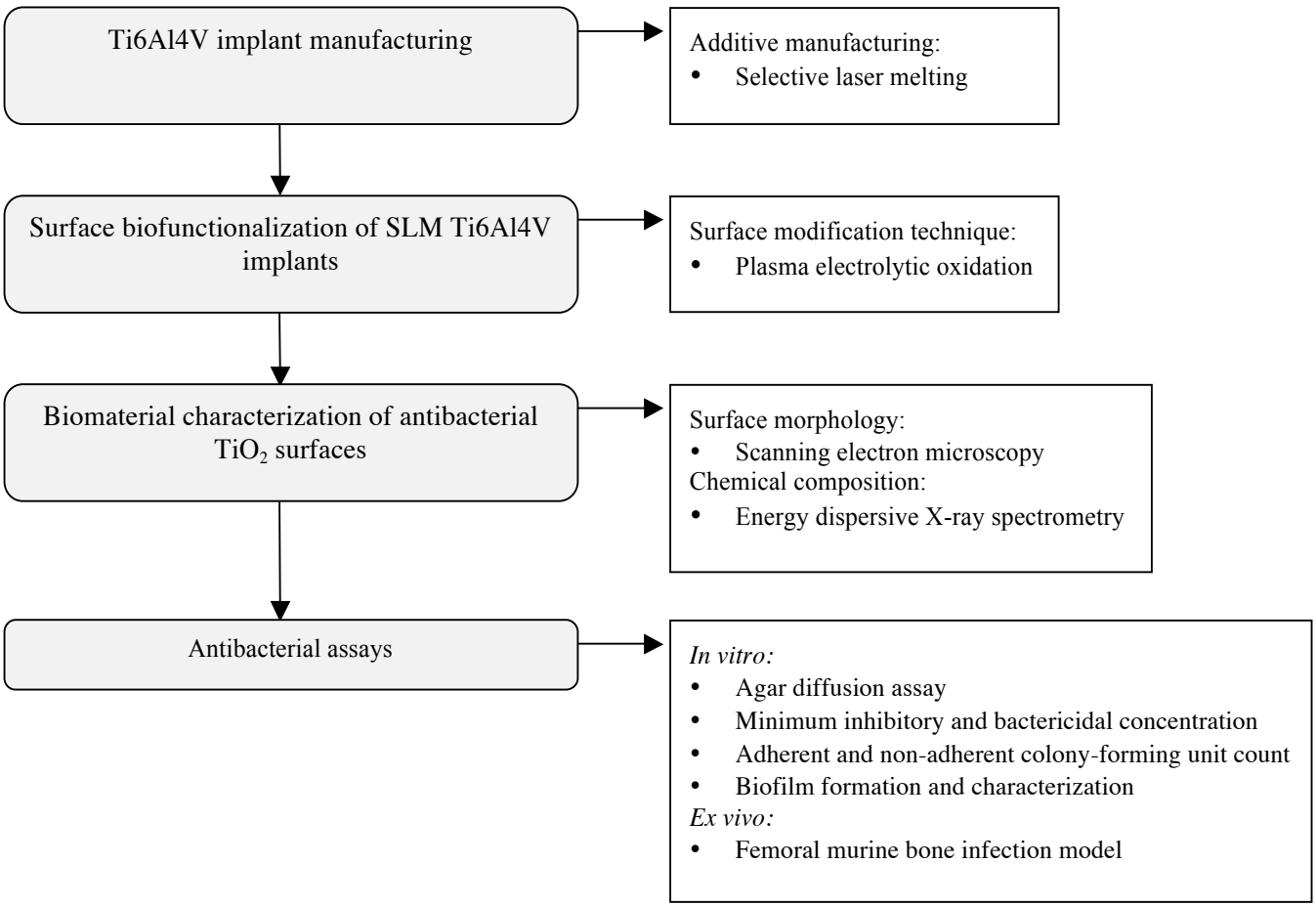

Fig. 1. Schematic representation of the study design

2.2 Selective laser melting Ti6Al4V implants

Medical grade porous SLM Ti6Al4V implants, designed and manufactured as previously described by [60], were used in this study. Implants of approximately 0.5 mm in diameter and 4 cm in length were manufactured in the Additive Manufacturing Lab (TU Delft, Delft, the Netherlands) by a SLM machine (SLM-125, Realizer, Borchem, Germany) with YLM-400-AC Ytterbium fiber laser (IPG Photonics Corporation, Oxford, United States). Prior to the SLM build process, parameters for laser processing were set. A laser power of 96 W, an exposure time of 300 μs and a wavelength of 1070 ± 10 nm were used. The bulk material used for the manufacturing of the implants was a medical grade (ELI, Class 23) Ti6Al4V powder (AP & C, Boisbriand, Quebec, Canada), with a spherical particle morphology and particle size distribution of 10 - 45 nm.

Post manufacturing, the as-manufactured implants were ultrasonically cleaned in acetone, 96% ethanol and subsequently demineralized water for 5 min each with a frequency of 50 - 60 Hz (Sonorex super Ultrasonic bath, Bandelin, Germany), to remove excess powder particles. Consecutively, the implants were dried in a stream of compressed air before undergoing PEO processing.

2.3 Surface biofunctionalization

2.3.1 Experimental PEO setup

PEO processing of the implants was conducted in the Surface Biofunctionalization Lab (TU Delft, Delft, The Netherlands) using a custom-made setup (Fig. 2A). The customized setup consisted of an AC power supply (50Hz, type ACS 1500, ET Power Systems Ltd., United Kingdom), a computer interfaced with the AC power supply connected via a data acquisition board (NI SCXI-1000, Austin, Texas, United States), a double-walled glass electrolytic cell with two electrodes configuration, connected to a thermostatic bath (Thermo Haake open-bath circulator V15, Thermo Fischer, USA) to preserve the temperature of the electrolytic cell during the PEO process, a magnetic stirrer and a thermometer. The two electrodes configuration refers to the implants ($n = 4$) as anode and a cylindrical shaped stainless steel as cathode.

2.3.2 Synthesis of antibacterial TiO_2 surface with Ag, Cu and Zn NPs

The PEO process was conducted in a double-walled glass electrolytic cell, filled with an electrolyte volume of 800 ml as previously described by [60] (Fig. 2B). The electrolyte consisted of 4.2 $g{\cdot}L^{-1}$ of calcium glycerophosphate (Dr. Paul Lohmann GmbH, Emmerthal, Germany) and 24 $g{\cdot}L^{-1}$ calcium acetate hydrate (Sigma-Aldrich, St. Louis, United States) dissolved in 800 ml demineralized water, to which various ratios of Ag NPs, Cu NPs and Zn NPs were dispersed (Table 1). The particle morphology and particle size distribution of the Ag NPs (Sigma-Aldrich, St. Louis, United States), pure Cu NPs (SkySpring Nanomaterials, Houston, USA) and pure Zn NPs (Sigma-Aldrich, St. Louis, United States), were spherical and 10 - 45 nm, 40 - 60 nm and 40 - 60 nm, respectively. After the dispersion of the NPs in the electrolyte, the electrolyte was sonicated twice in an ultrasonic bath (Bandelin Sonorex, Bandelin Electronic, Berlin, Germany) for 5 min to acquire a homogenous dispersion. In-between, the electrolyte was stirred for 5 min by a magnetic stirrer (40 x 8 mm, VWR, Radnor, Pennsylvania, USA) at 500 rotations per min (rpm).

Four implants were connected to a metal rod and completely submerged in the center of the double-walled glass electrolytic cell in the electrolyte. A cylindrical stainless steel cathode was situated against the internal wall of the electrolytic cell, completely surrounding the anode. Prior to the process, the electrolyte temperature was kept constant at 5 ± 1 °C, using the thermostatic bath. The process was conducted under galvanostatic conditions, with a current density of 20 A/dm^2, applied by the AC power supply. The duration of the PEO process was 300 s. A homogeneous particle distribution was maintained by stirring the electrolyte constantly at 500 rpm.

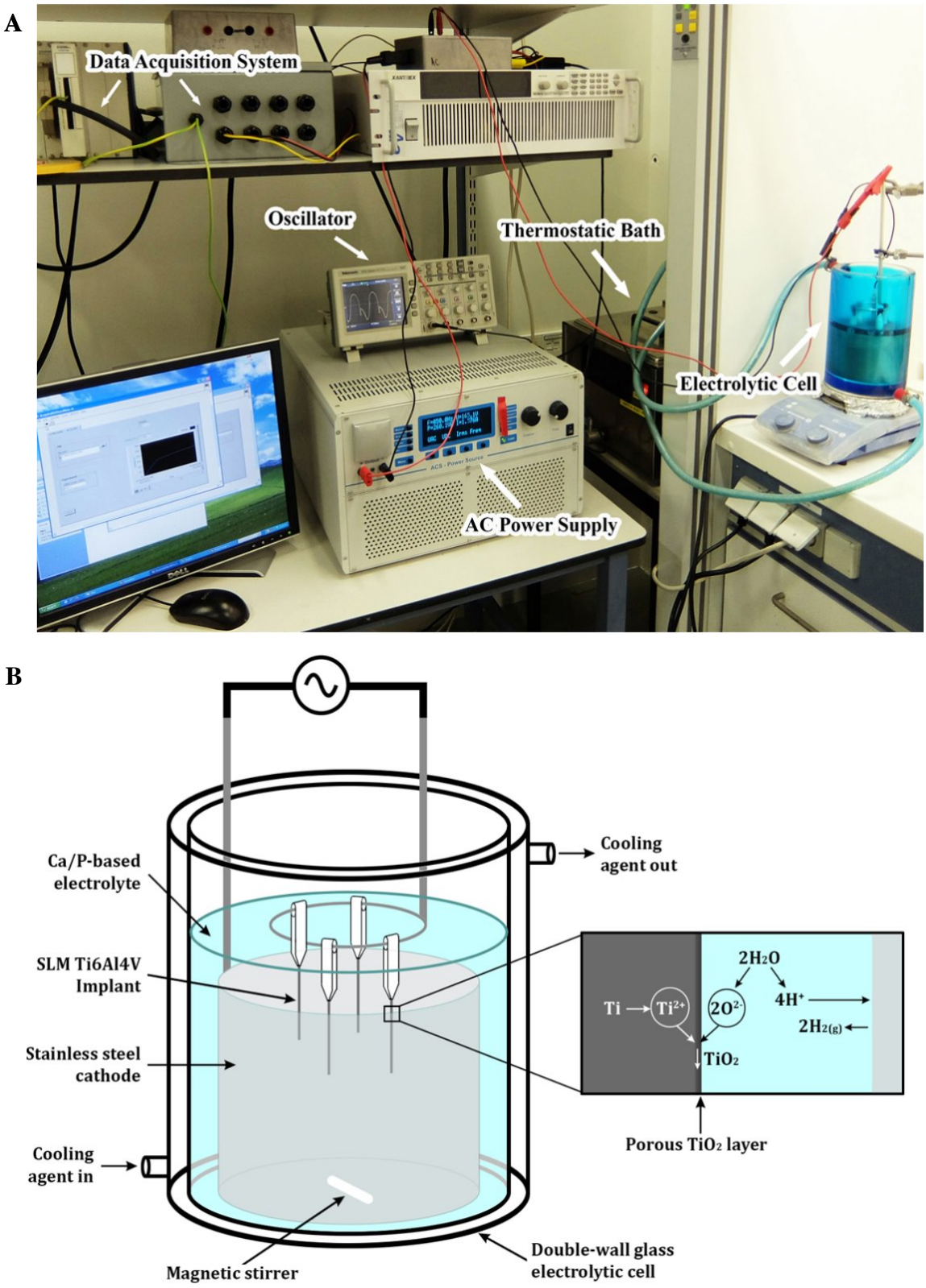

Fig. 2. Schematic representation of the custom-made setup for the PEO process. (A) The customized setup consisted of an AC power supply, data acquisition system, oscillator, double-walled glass electrolytic cell and thermostatic bath [61]. (B) Schematic representation of the double-walled glass electrolytic cell, adapted from [62].

The voltage-time (V-t) transients were recorded with a sampling rate of 1 Hz during the process. To remove residual electrolyte and non-attached NPs, the treated implants were rinsed in flowing tap water for 1 min after the PEO process and dried successively with compressed air. Prior to biomaterial characterization and *in vitro* and *ex vivo* antibacterial assays, all implants were cut to a length of approximately 1 cm and sterilized for 15 min at 121 °C using a Sanamij autoclave.

Moreover, a set of implants was processed by PEO without the dispersion of NPs in the electrolyte (PT), serving as process controls, to separate the effects of the NPs from those of the PEO process. Additional controls were implants without any surface modification treatment (NT). An outline of the experimental groups and compositions of the electrolyte used for the PEO process are listed in Table 1.

Table 1.
Outline of the experimental groups (group codes) and compositions of the PEO electrolytes, used to synthesize the experimental groups.

Experimental groups	Electrolyte components				
	Calcium acetate, $g \cdot L^{-1}$	Calcium glycero-phosphate, $g \cdot L^{-1}$	Ag NPs, $g \cdot L^{-1}$	Cu NPs, $g \cdot L^{-1}$	Zn NPs, $g \cdot L^{-1}$
Non-treated (NT)	0	0	0	0	0
PEO-treated (PT)	24	4.2	0	0	0
PT - Ag	24	4.2	3	0	0
PT - Ag 75	24	4.2	2.25	0	0
PT - Ag 50	24	4.2	1.5	0	0
PT - Ag 25	24	4.2	0.75	0	0
PT - Ag Cu	24	4.2	3	3	0
PT - Ag Cu 75 25	24	4.2	2.25	0.75	0
PT - Ag Cu 50 50	24	4.2	1.5	1.5	0
PT - Ag Cu 25 75	24	4.2	0.75	2.25	0
PT - Cu	24	4.2	0	3	0
PT - Ag Zn	24	4.2	3	0	3
PT - Ag Zn 25 75	24	4.2	2.25	0	0.75
PT - Ag Zn 50 50	24	4.2	1.5	0	1.5
PT - Ag Zn 75 25	24	4.2	0.75	0	2.2.5
PT - Zn	24	4.2	0	0	3

2.4 Biomaterial characterization

2.4.1 Scanning electron microscopy (SEM)

The morphology and structure of the surface of the implants after biofunctionalization and after *in vitro* antibacterial assays were explored using a scanning electron microscopy (SEM), a JSM-IT100 (JEOL, Tokyo, Japan) microscope. Electron beam energy of 5 - 20 kV and a working distance of 10 mm were used. Prior to investigation, the implants (n = 3/group) were first cleaned in acetone and then in 2-propanol (Sigma-Aldrich) for 30 s each. In addition, the implants were coated with a gold layer of 5 ± 2 nm to ensure good electrical conduction.

2.4.2 Energy dispersive X-ray spectroscopy (EDS)

The presence of NPs in the surface of the implants was examined by energy dispersive X-ray spectroscopy (EDS), revealing the chemical composition of specific selected areas on the surface by spot analysis.

2.5 Antibacterial assays

2.5.1 Preparation of bacterial inoculum

One colony of MRSA strain USA300, from a streak plate, was suspended in 3 ml tryptic soy broth (TSB, UMC Utrecht, Utrecht, the Netherlands) and incubated for 2 - 3 h at 37 °C, shaking at 120 rpm. After incubation, the optical density of the suspension at 600 wavelengths (OD_{600}) was measured by a spectrophotometer (Genesys Thermospectronic, Thermo Fisher Scientific, Waltham, USA). Based on the measured OD_{600}, the suspension was diluted to the desired bacterial inoculum using phosphate-buffered saline (PBS, UMC Utrecht, Utrecht, the Netherlands). All implants used in the antibacterial assays were of approximately 0.5 mm in diameter and 1 cm in length.

2.5.2 Bacterial inoculum check

The desired bacterial inoculum was checked by a quantitative culture. Ten-fold serial dilutions of the stock bacterial inoculum were prepared and successively plated onto blood agar plates, by pipetting aliquots of 10 μl of the ten-fold serial dilution ($10e^{0}$ – $10e^{-6}$). The blood agar plates were incubated overnight at 37 °C and colony-forming units (CFU) were quantified the following day.

2.5.3 *In vitro* assays

2.5.3.1 Agar diffusion assay

To investigate the *in vitro* leachable antibacterial activity of the implants, a modified agar diffusion assay was conducted (Fig. 3). Briefly, Luria-Bertani (LB) agar plates were prepared by boiling solid LB nutrient medium (UMC Utrecht, Utrecht, The Netherlands) in a microwave. Subsequently, aliquots of 2 ml were poured into sterilized petri dishes and stored at room temperature, to allow the LB agar to solidify. After solidification, a sterile cotton swab was used to distribute the suspension containing 10^{7} CFU/ml of MRSA USA300 equally on the agar surface (Fig. 3A). The agar plates were rotated 90° with each sweep (Fig. 3B), until the plates were rotated 360°, and the agar surface was fully inoculated. After 3 min of absorption, three implants were placed side by side onto the inoculated agar surface and incubated for 24 h at 37 °C, to allow bacterial growth (Fig. 3C). After incubation, the *in vitro* leachable antibacterial activity was determined by measuring the surface area of the colorless inhibition zones (Fig. 3D). To quantify the zones, the agar plates were photographed by Image Quant LAS 4000 (GE Healthcare Bio-Sciences, Björkgatan, Sweden) and transferred to an image processing software (ImageJ, National Institutes of Health Maryland, USA), to quantify the area of the inhibition zones in cm^{2}. The experiments were performed simultaneously for three implants of each experimental group (n = 3/group) and the average surface area was recorded.

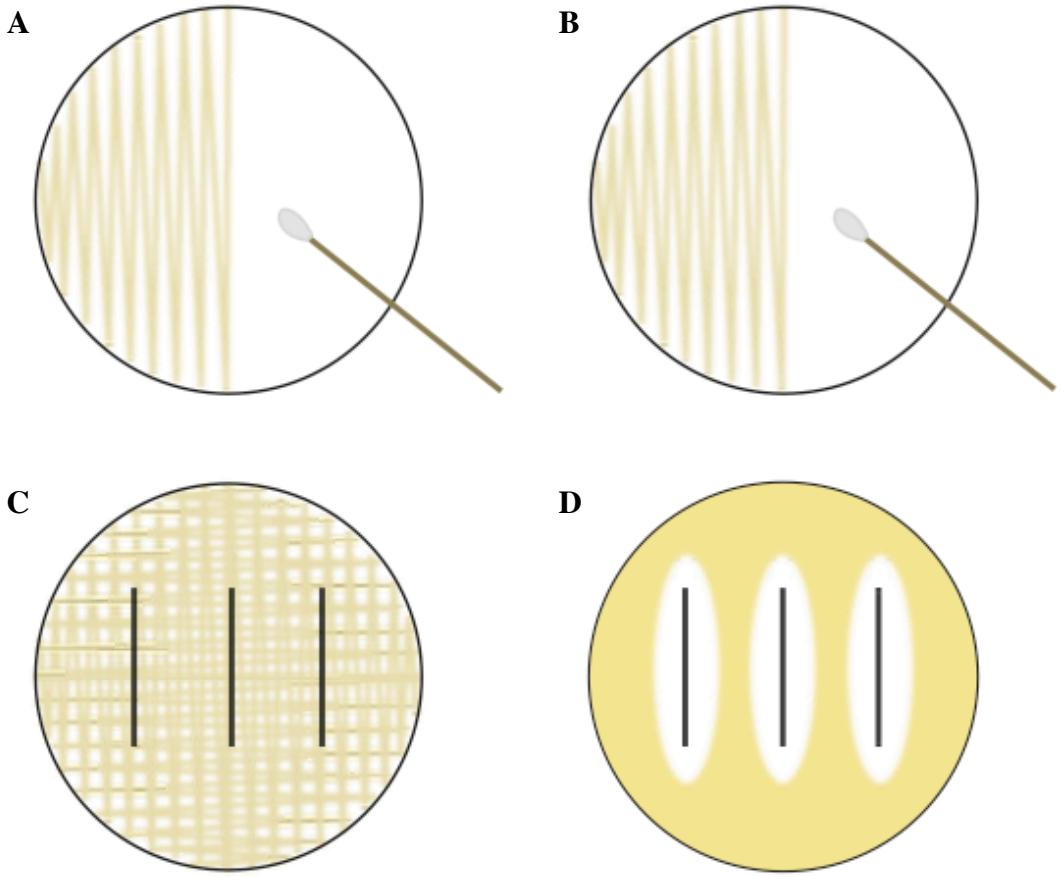

Fig. 3. Agar diffusion assay for assessment of leachable antibacterial activity by implants. (A) A MRSA inoculum was equally distributed on the LB-agar plate using a cotton swab. (B) The plates were rotated 90° with each swab, until the plates were rotated 360°. (C) After absorption, three identical implants were placed side by side onto the agar surface. (D) After 24 h of incubation at 37°C, the leachable antibacterial activity of the implants was determined by measuring the surface area of the colorless inhibition zones. Bacterial growth was indicated by a color change. Image created using GravitDesigner for Mac IOS (Gravit GmbH, Nuremberg, Germany).

2.5.3.2 Minimum inhibitory and bactericidal concentration

The minimum inhibitory and bactericidal concentrations (MIC and MBC, respectively) of Ag^{+}, Cu^{2+} and Zn^{2+} ions, as well the combinations, were determined by a micro-dilution assay (Fig. 4). The $AgNO_3$, $Cu(NO_3)_2$ and $Zn(NO_3)_2$ dissolved in Cation-Adjusted Mueller Hinton broth (CAMH, UMC Utrecht, Utrecht, The Netherlands) were diluted to the highest concentrations to be examined (0.125, 80 and 80 mM, respectively). Sequentially, serial two-fold dilutions suspensions were prepared over a range of 0.125 to 0.00024 mM, 80 to 0.04 mM and 80 to 0.04 mM, respectively, in 96-well micro-titration plates (Fig. 4A). Individual wells of round-bottom 96-well micro-titration plates were filled with aliquots of 50 μl of the serial two-fold dilutions (Fig. 4B) and inoculated sequentially with 50 μl of 0.9 x 10^8 CFU/ml of MRSA USA300 (Fig. 4C). After well mixing (Fig. 4D), the inoculated 96-well micro-titration plates were incubated overnight at 37 °C, static. After 24 h of incubation, the growth inhibition was visually determined using an inverted magnifying mirror. Bacterial growth was characterized by visual turbidity and growth inhibition resulted in wells not visibly turbid. MICs were determined as the lowest concentration that resulted in inhibition of bacterial growth, i.e. not visual turbid (Fig. 4E).

After MIC determination, subcultures from the wells not visibly turbid were prepared by pipetting 10 µl of the wells onto blood agar plates (Fig. 4F). The blood agar plates were incubated for 24 h at 37 °C and visually inspected for bacterial growth the following day. MBCs were determined as the lowest concentration that resulted in no bacterial growth (CFUs) on subcultures.

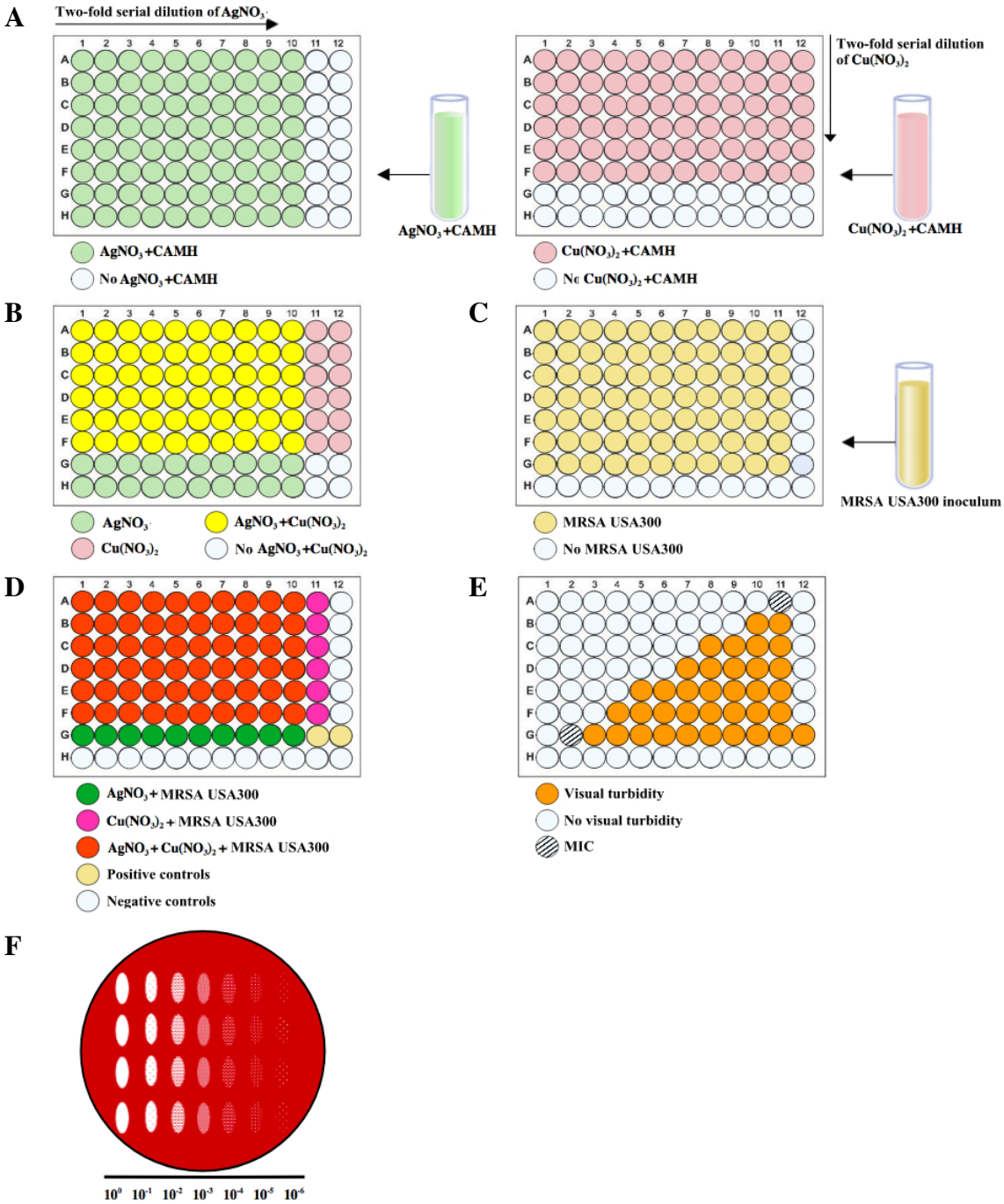

Fig. 4. Micro-dilution assay to determine the minimum inhibitory and bactericidal concentration. (A) Serial two-fold dilutions were prepared for $AgNO_3$ and $Cu(NO_3)_2$. (B) 50 µl of the serial two-fold dilutions were pipetted in the 96-well micro-titration plates (C) Inoculation with 50 µl of 0.9 x 10^8 CFU/ml of MRSA USA300. (D) The bacterial inoculum and antibacterial agents were mixed. (E) After static incubation for an incubation period of 24 h at 37 °C, the MIC was visually determined as the lowest concentration that resulted in no visual bacterial growth. (F) To determine the MBC, 10 µl of the wells not visible turbid were pipetted onto blood agar plates. The MBCs were determined as the lowest concentration that resulted in no CFU growth after incubation overnight. Image created using GravitDesigner for Mac IOS (Gravit GmbH, Nuremberg, Germany).

2.5.3.3 Adherent and non-adherent colony-forming unit count

The bactericidal properties of the implants against MRSA USA300 were assessed *in vitro* by quantifying the surface-adherent and non-adherent bacteria after 24 h of culture (Fig. 5). Four implants were inoculated by immersion in 100 µl of TSB, containing 1% glucose and 2 x 10^2 CFU of MRSA USA300 and incubated overnight at 37 °C, static (Fig. 5A). After incubation, the implants were extracted from the medium cultured and washed three times in PBS, to remove residuary non-adherent bacteria from the implant surface. The culture medium was used, to determine the viable counts of non-adherent bacteria. After that, the implants were situated in 2ml of PBS and sonicated, to detach the surface-adherent bacteria (Fig. 5B). After sonication, ten-fold serial dilutions of the sonicates and culture medium were prepared in duplo and plated onto blood agar plates by pipetting aliquots of 10 µl of the ten-fold serial dilutions ($10e^0$ – $10e^{-6}$) (Fig. 5C). The blood agar plates were incubated for 24 h at 37 °C and the viable CFUs were quantified the following day. For quantification, the blood agar plates were photographed by Image Quant LAS 4000 and analyzed using Matlab r2017b (Version 9.3, MathWorks, Natick, Massachusetts, United States). The experiments were performed simultaneously for three implants of each experimental group (n = 3/group) and the average count of viable CFUs was recorded

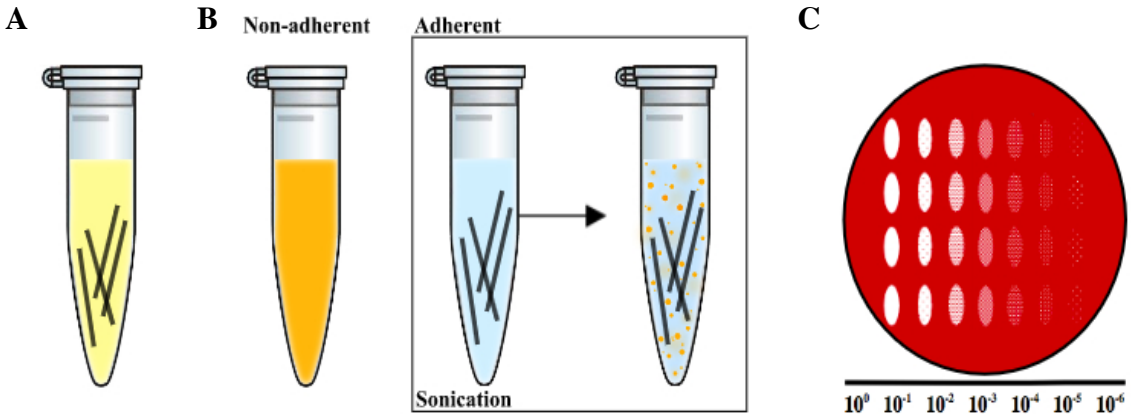

Fig. 5. Antibacterial assay to determine the bactericidal properties of the implants. (A) Four implants were inoculated with 2 x 10^2 CFU of MRSA USA300 dissolved in TSB and 1% glucose. (B) After 24 h of incubation at 37 °C, the implants were extracted from the medium, washed and situated in 2ml of PBS and sequentially sonicated, to detach surface-adherent bacteria. The culture medium was used, to determine the viable counts of non-adherent bacteria. (C) Ten-fold serial dilutions of sonicates and culture medium were pipetted onto blood agar plates in duplo. The blood agar plates were incubated for 24 h at 37 °C and the viable CFUs were quantified the following day. Image created using GravitDesigner for Mac IOS (Gravit GmbH, Nuremberg, Germany).

2.5.3.4 Biofilm formation and characterization

The anti-biofilm properties of the implants were investigated using SEM. The implants were inoculated by immersion in 100 µl of TSB, containing 1% glucose and 2 x 10^2 CFU of MRSA USA300 and incubated overnight at 37 C°, static. After incubation, the implants were fixed in 600 µl of McDowels fixative, which had been pipetted and stored in 0.5 ml Eppendorf tubes. The McDowels fixative agent consisted of 10 mM of PBS, containing 1% glutaraldehyde (UMC, Utrecht, The Netherlands) and 4% paraformaldehyde (Alfa Aesar, Karlsruhe, Germany), at pH 7.4. Prior to SEM investigation, the implants were rinsed for 10 min in demineralized water and dehydrated afterwards. The dehydration process consisted of an immersion

in 50%, 70% and 96% ethanol and successively in hexamethyldisilazane (Sigma-Aldrich, St. Louis, Missouri, USA), for 15, 20, 20 and 30 min, respectively. The implants were then air-dried for 2 h and subsequently coated with a gold layer of 5 ± 2 nm to ensure good electrical conduction. The experiments were performed for one implant from each experimental group (n = 1/ group).

2.5.4 *Ex vivo* assay in femoral murine infection model

To investigate the *ex vivo* antibacterial properties of the implants, a femoral murine infection model was utilized (Fig. 6). The Common Animal Laboratory of the University Utrecht (UU) (Utrecht, The Netherlands) provided the femurs from murine cadavers type C57BI/6. Prior to the *ex vivo* implantation procedure (Fig. 6), adhesive soft tissue was removed from the femur using a surgical scalpel and sequentially sterilized in 70% ethanol and immersed in demineralized water for 10 min each, to remove residual quantities of ethanol. After the sterilization procedure, a hole was drilled into the epicondyle of the femur using a 0.5 mm drill (RISystem, Davos, Switzerland), to insert the implant into the intramedullary canal. The drill was positioned onto the epicondyle at an angle of 45° and the angle decreased to 0° with respect to the longitudinal axial axis of the femur during drilling (Fig. 6A). Sequentially, bone marrow was purged from the bone cavity using a syringe and 20 μl of PBS was injected, to mimic the *in vivo* environment (Fig. 6B). Prior to implantation, the implants were inoculated through distribution of 2 μl of PBS with 2 x 10^2 CFU of MRSA USA300 onto the implant surface using a pipette tip (Fig. 6C). The implants were then air-dried for 30 min and implanted into the femur by applying a slight pressure (Fig. 6D). After that, the femurs were located in 0.5 ml Eppendorf tubes and incubated overnight at 37 °C. The process was performed dynamically, to stimulate the intraosseous fluid flow.

To validate the *ex vivo* femoral murine infection model, the bone cavity of one femur was injected with 20 µl of tetracycline hydrochloride (50 mg/ml, Sigma-Aldrich), an active antibiotic against MRSA [63], before receiving an inoculated NT implant (NT - tetra). In addition, one femur was not implanted with an inoculated implant to validate the sterilization procedure of the femurs (negative control).

After incubation, the femurs were immersed in 800 μl of PBS and 15 beads of zirconium oxide (Ø 2 mm, BioSpec, Bartlesville, Oklahoma, USA) were added. Subsequently, a MagNA Lyser (Roche Diagnostics, Risch-Rotkreuz, Switzerland) was used, to homogenize the femurs, by two cycles of 30 s at 7000 rpm (Fig. 6E). In-between the cycles, the homogenates were cooled on ice for 30 s. Ten-fold serial dilutions of the homogenates were prepared in duplo and plated onto blood agar plates by pipetting aliquots of 10 µl of the ten-fold serial dilutions ($10e^0$ – $10e^{-6}$) (Fig. 6F). The blood agar plates were incubated for 24 h at 37 °C and the viable CFUs were quantified the following day. For quantification, the blood agar plates were photographed by Image Quant LAS 4000 and analyzed using Matlab r2017b. The *ex vivo* experiments were performed simultaneously for three implants of the NT, PT, PT – Ag, PT – Ag 50, PT – Ag Cu, PT – Ag Cu 75 25, PT – Ag Zn and PT - Ag Zn 75 25 implants (n = 3/group). The average count of viable CFUs was recorded

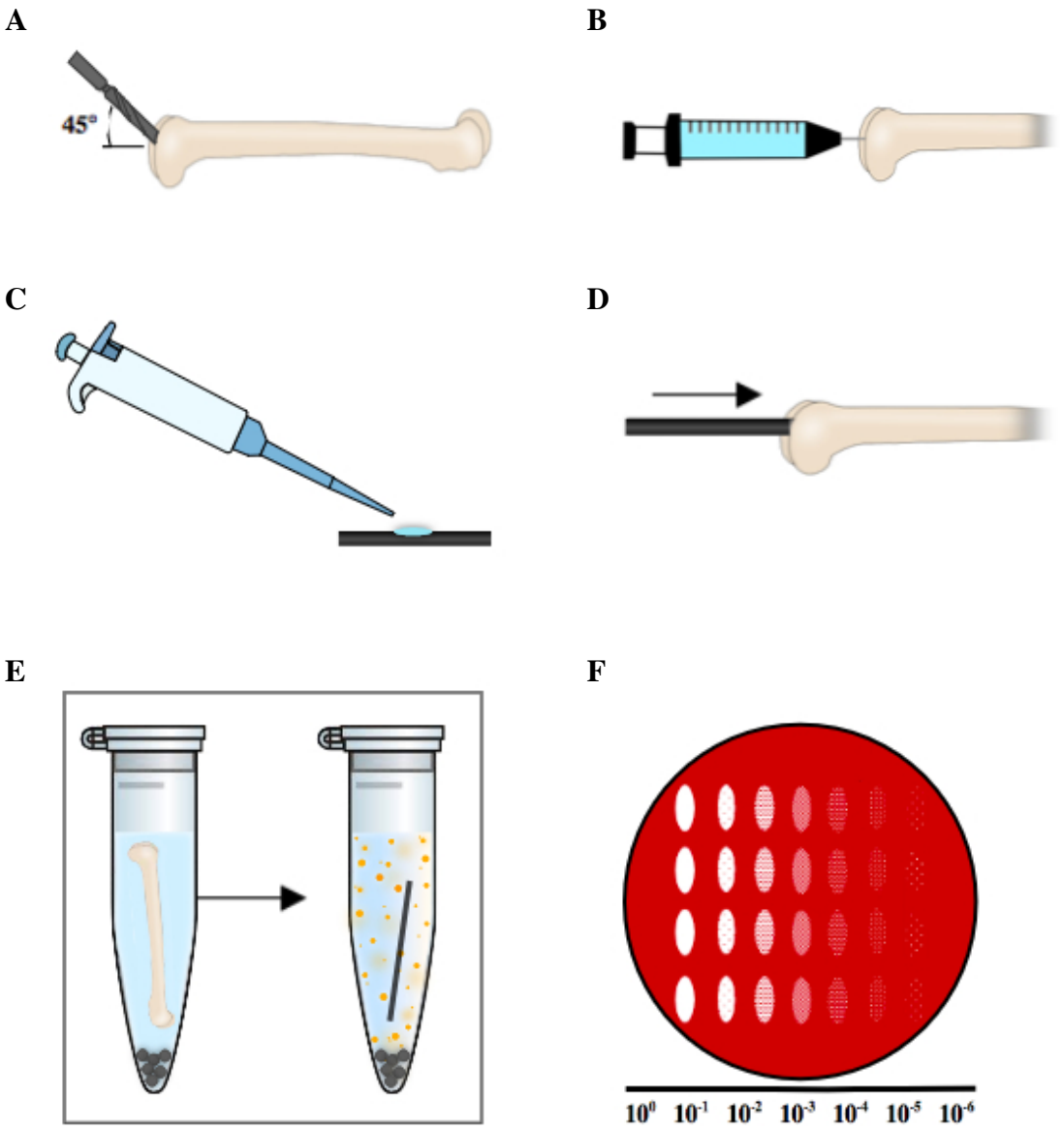

Fig. 6. Femoral murine infection model for assessment of *ex vivo* antibacterial properties of the implants. (A) A hole was drilled into the epicondyle of the femur. The drill was positioned at an angle of 45° and decreased to 0° during drilling. (B) Bone marrow was purged using a syringe and 20 μl of PBS was injected. (C) Implant was inoculated with 2 x 10^2 CFU of MRSA USA300 onto the implant surface using a pipette tip. (D) Implant was implanted into the femur by applying pressure. (E) After an incubation period of 24 h at 37 °C, the femur was immersed in PBS and homogenized using a MagNA Lyser. (F) Ten-fold serial dilutions of the homogenate were pipetted onto blood agar plates in duplo and incubated overnight at 37 °C. The viable CFUs were quantified the following day. Image created using GravitDesigner for Mac IOS (Gravit GmbH, Nuremberg, Germany), modified from [64].

2.6 Statistical analysis

Data was expressed as mean ± standard deviation (SD). The statistical analysis was performed with IBM SPSS Statistics Version 23 for Mac IOS (SPSS Software, Armonk, NY, United States) using one-way ANOVA. The differences between experimental groups were considered statistically significant at $p < 0.05$.

3 Results

3.1 Surface biofunctionalization and characterization

3.1.1 Voltage-time transients recorded during PEO

The surfaces of the SLM Ti6Al4V implants were biofunctionalized by PEO, for the synthesis of an antibacterial TiO_2 surface layer with various ratios of Ag NPs, Cu NPs and/or Zn NPs. During the process, the V-t transients were recorded for the experimental groups. In general, the V-t transients showed equivalent characteristics (Fig. 7). An initial increase in oxidation voltage was observed for all experimental groups in the recorded V-t transients for about 9 ± 1 s. The rate of initial increase varied between 13.0 ± 2.2 V/s and 13.8 ± 2.5 V/s (Table 2). No significant differences were observed in the rate of initial voltage increase between the experimental groups. After 9 ± 1 s, plasma discharge was initiated, characterized by the bending of the slopes of the V-t transients. This indicated that the dielectric breakdown occurred i.e. the formation of pores. The dielectric breakdown occurred at voltages between 110.4 ± 2.8 V and 117.0 ± 3.7 V (Table 2). No significant differences were observed in the dielectric breakdown voltage between the experimental groups. After approximately 180 s, the oxidation voltage increased linearly until the oxidation time of 300 s was reached. The final oxidation voltages after 300 s were observed in the range of 227.6 ± 0.3 and 249.5 ± 1.3 V (Table 2). Significant differences were observed in recorded final oxidation voltages. The addition of Ag NPs to Cu NPs and Zn NPs caused a significantly lower final oxidation voltage ($p < 0.01$), as compared to only Cu NPs and Zn NPs.

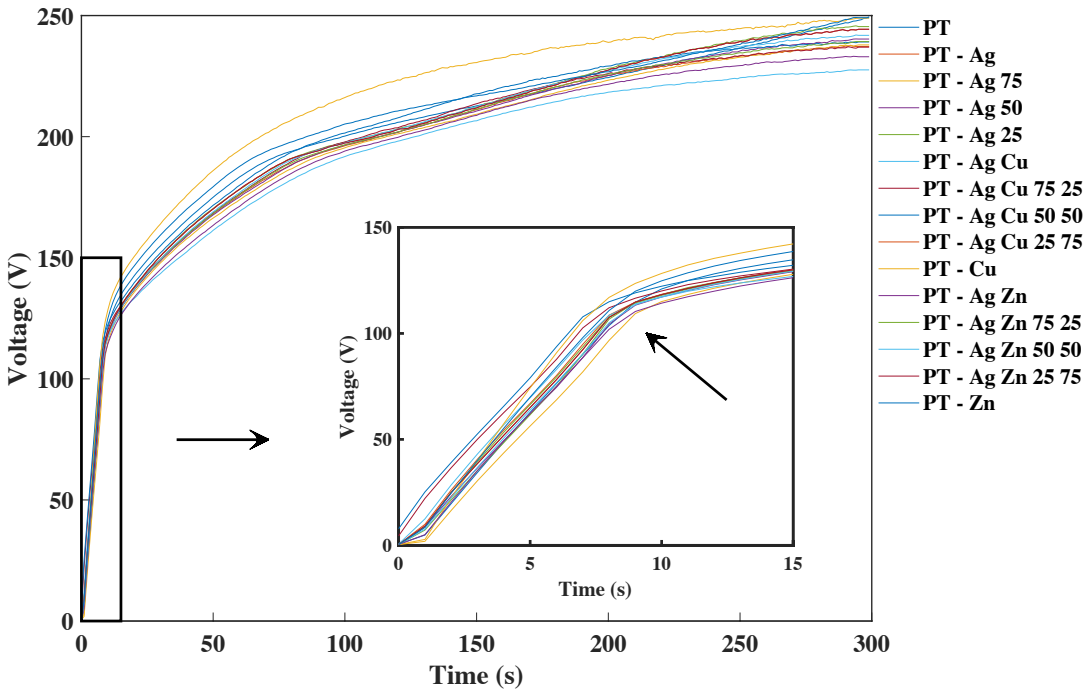

Fig. 7. Average V-t transients recorded during PEO process. Black arrow indicated dielectric breakdown. $N = 4$/group.

Table 2.
Process parameters obtained during PEO process. *N* = 4/group.

Experimental groups	Process parameters		
	Initial rate, V/s	Dielectric breakdown, V	Finale voltage, V
PT	13.7 ± 1.2	114.7 ± 4.5	249.5 ± 1.3
PT - Ag	13.5 ± 1.9	114.8 ± 1.4	237.2 ± 2.3
PT - Ag 75	13.4 ± 0.9	115.0 ± 2.3	237.9 ± 2.7
PT - Ag 50	13.0 ± 2.2	113.3 ± 0.9	240.3 ± 1.9
PT - Ag 25	13.4 ± 2.4	114.7 ± 0.4	245.4 ± 2.2
PT - Ag Cu	13.5 ± 1.4	114.0 ± 0.5`	227.6 ± 0.3
PT - Ag Cu 75 25	13.5 ± 2.4	112.1 ± 0.9	236.9 ± 0.5
PT - Ag Cu 50 50	13.4 ± 2.9	114.9 ± 1.7	239.1 ± 0.1
PT - Ag Cu 25 75	13.4 ± 1.9	111.8 ± 2.4	240.0 ± 0.7
PT - Cu	13.7 ± 5.8	117.0 ± 3.7	248.9 ± 2.5.
PT - Ag Zn	13.8 ± 1.0	110.4 ± 2.8	233.0 ± 1.2
PT - Ag Zn 75 25	13.4 ± 2.3	114.4 ± 1.2	239.3 ± 1.7
PT - Ag Zn 50 50	13.1 ± 2.5	113.5 ± 2.3	241.8 ± 1.6
PT - Ag Zn 25 75	13.4 ± 2.1	114.8 ± 0.3	244.3 ± 0.3
PT - Zn	13.8 ± 2.5	110.8 ± 2.1	249.1 ± 0.8

3.1.2 Surface morphology and chemistry of the biofunctionalized implants

The morphology and structure of the surface of the implants after biofunctionalization, were investigated using SEM, in particular of the PT, PT - Ag, PT - Cu and PT - Zn implants. Low magnification SEM images (secondary) revealed that a typical PEO morphology had been developed, because a uniform and homogeneous micro-/nano-porous oxide layer covered the entire surface of the implants (Fig. 8). In addition, well-separated interconnected pores, varying in size from a couple of nm to 5 μm, were distributed homogeneously across the surface of the implants (Fig. 8, right). No morphological differences were observed between the experimental groups.

Moreover, high magnification secondary and backscattered SEM images showed the presence of Ag NPs, Cu NPs and Zn NPs in the TiO_2 surface layer and distributed homogeneously over the surface, while no NPs were observed on the surface of the PT implant (Fig. 9). Moreover, the presence of NPs in the surface of the implants was chemically confirmed by EDS spot analysis. The EDS spot analysis detected Ca, P, Ti, Al, V, O, C elements in the surface of the implants (Fig.10). In addition, NPs were detected in the surface of the PT - Ag, PT - Cu and PT - Zn implants (Fig.10B,C and D). The Ti, Al and V are the alloying elements of the Ti6Al4V implant substrate, whereas the NPs, Ca/P-based species originated from the PEO electrolyte.

Comprehensive analysis of the surface morphology, structure and chemistry of implants with various ratios of Ag NPs, Cu NPs and/or Zn NPs have been previously reported in [62] and [65] and therefore excluded in the current study.

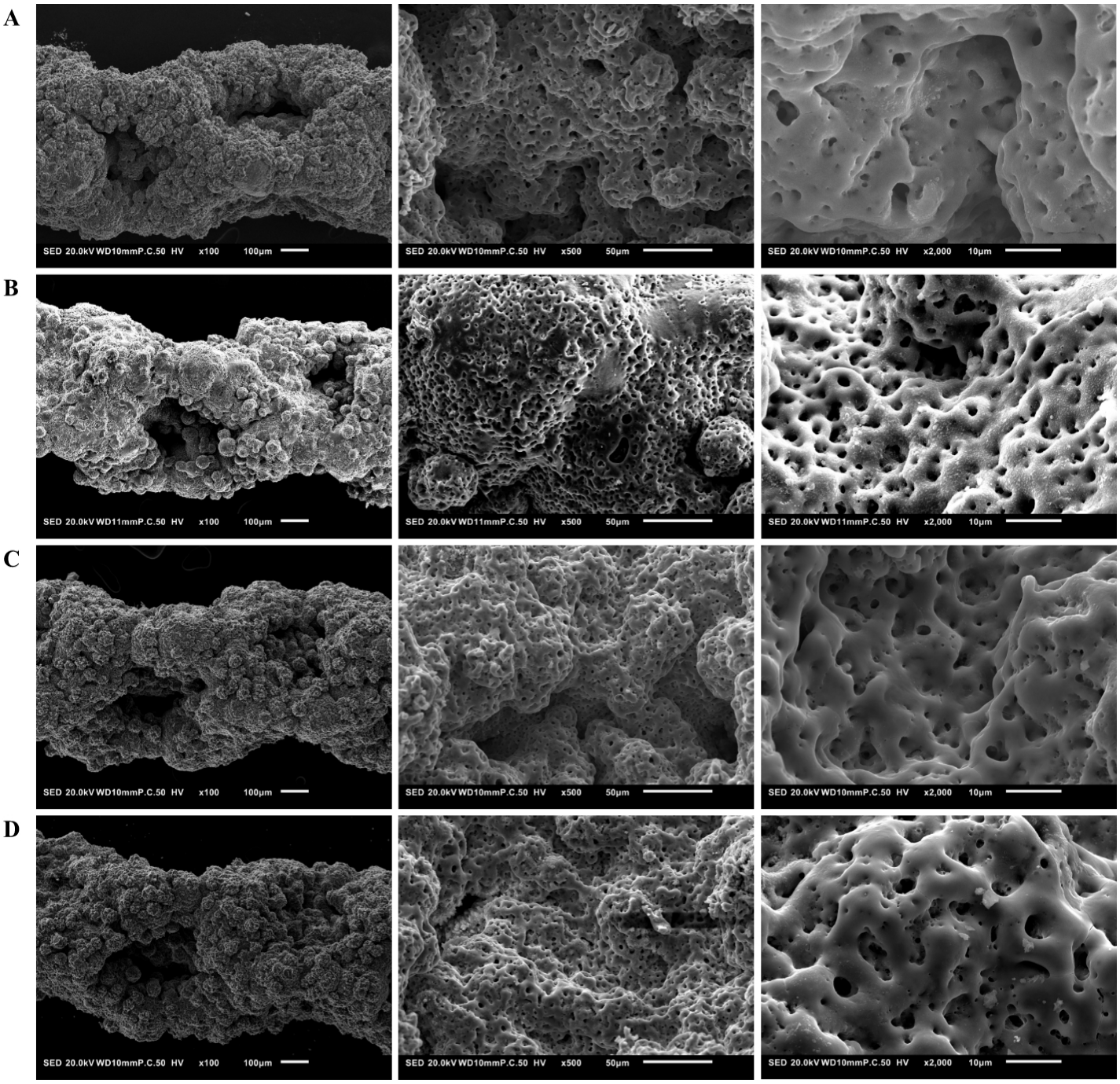

Fig. 8. Low (100 - 2000x) magnification SEM images (secondary) of the surface of the (A) PT, (B) PT - Ag, (C) PT - Cu and (D) PT – Zn implants.

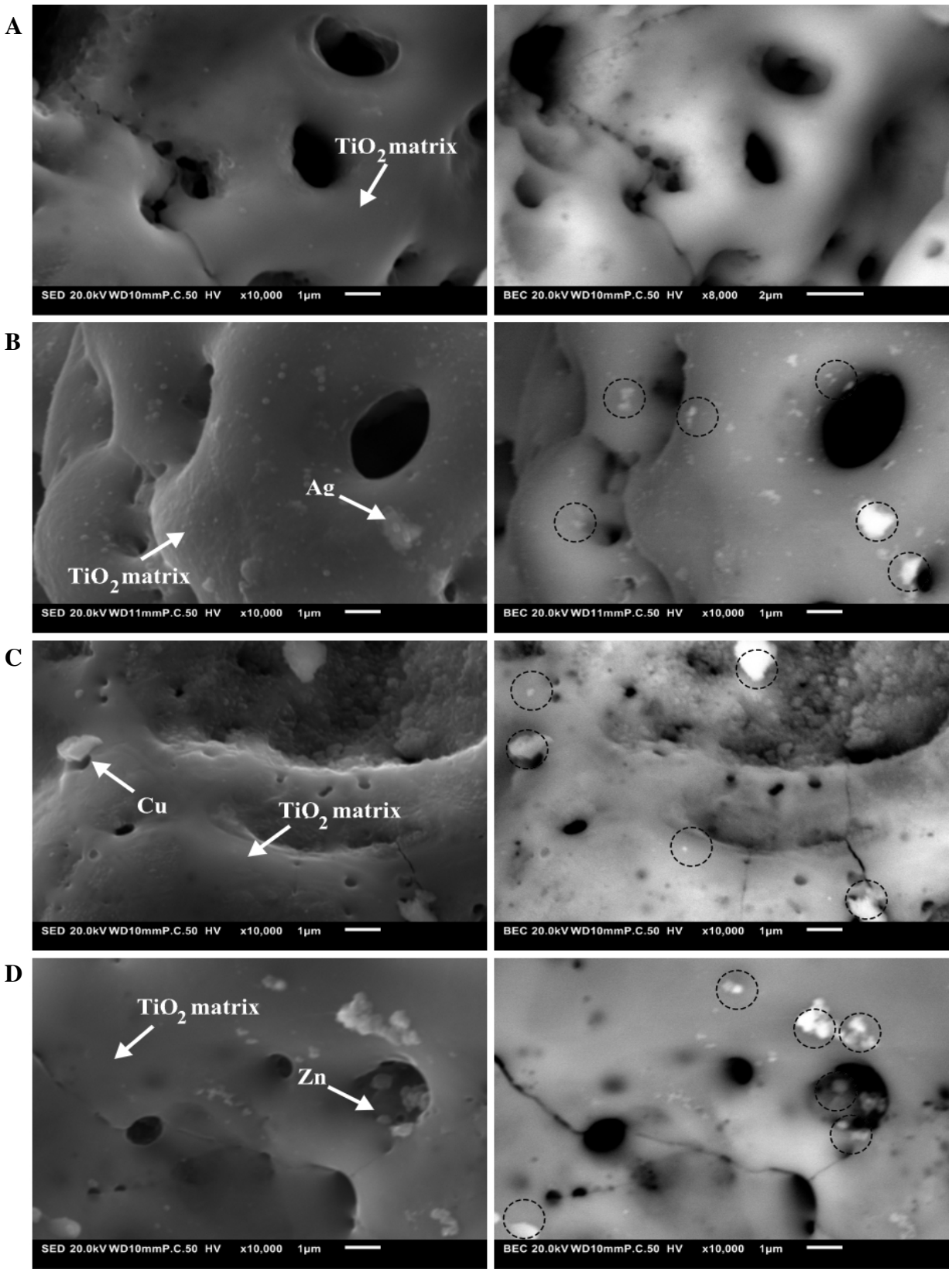

Fig. 9. High (10.000x) magnification SEM images of the surface of the (A) PT, (B) PT - Ag, (C) PT - Cu and (D) PT – Zn implants. Secondary (left) and backscattered (righ). The dotted circles represented the locations of NPs.

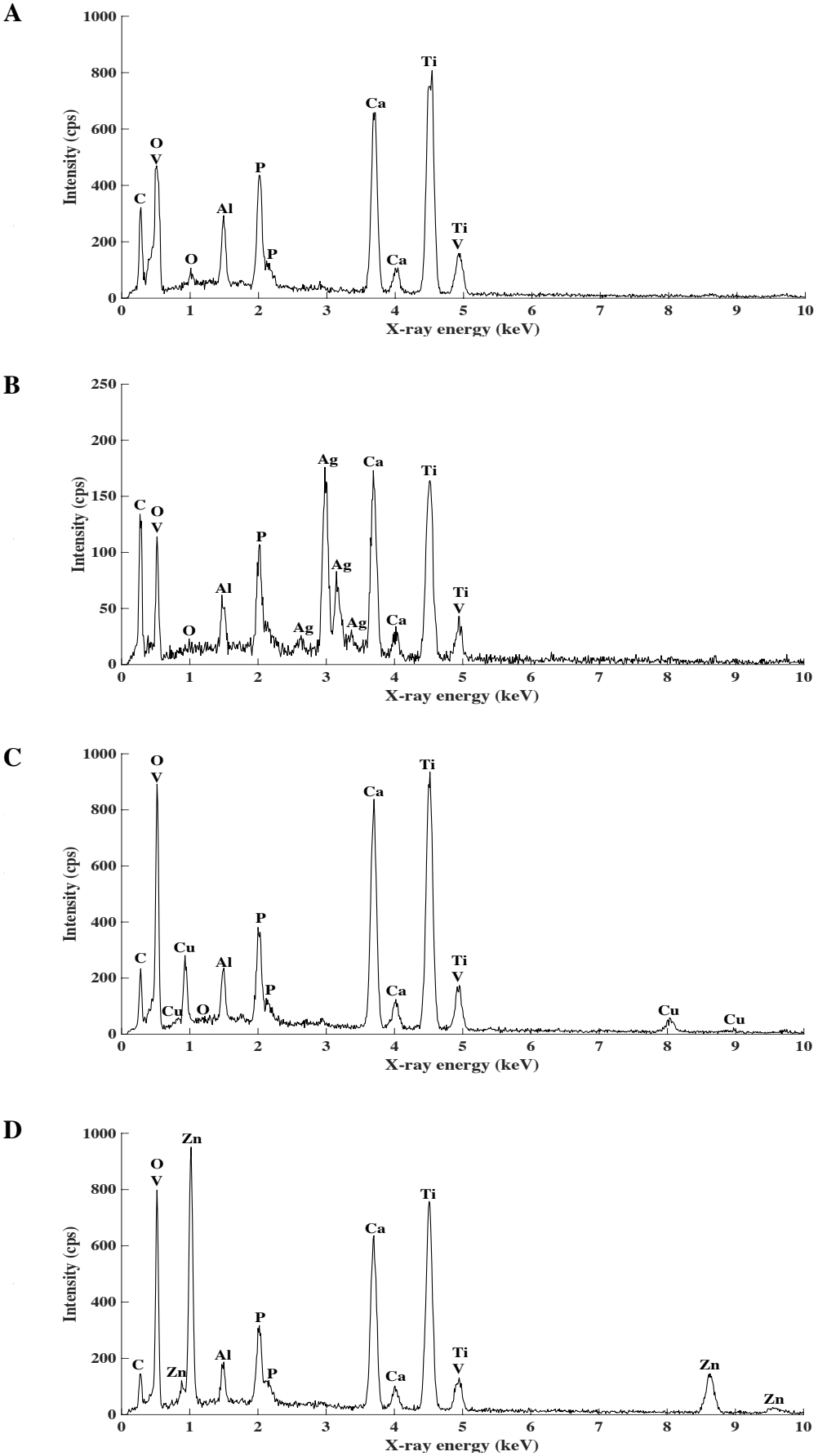

Fig. 10. EDS spectra of selected area of the surface of the (A) PT, (B) PT - Ag, (C) PT - Cu and (D) PT – Zn implants.

3.2 Antibacterial experiments

3.2.1 *In vitro* antibacterial activity of the implants

3.2.1.1 Leachable antibacterial activity, inhibition zones

The *in vitro* leachable antibacterial activity of the implants against MRSA was assessed using a modified agar diffusion assay. After an incubation period of 24 h, colorless inhibition zones were shown around all implants with NPs, except for PT - Cu and PT - Zn implants. Smaller zones were observed at the edges of the implants as compared to the zones along the longitudinal axial axis of the implants. No inhibition zones were demonstrated for the NT, PT, PT – Cu and PT - Zn implants (Fig.11A).

Quantification demonstrated comparable inhibition zones around the implants among PT – Ag, PT – Ag 75, PT – Ag 50, PT – Ag 25, PT – Ag Cu, PT – Ag Cu 75 25, PT – Ag Cu 50 50, PT – Ag Cu 25 75, PT – Ag Zn 75 25, PT – Ag Zn 50 50, PT – Ag Zn 25 75 implants. The results demonstrated that substitution of the content of Ag NPs partly with Cu NPs or Zn NPs does not affect the antibacterial leaching activity. Substitution of Cu NPs or Zn NPs contents with Ag NPs enhanced the leaching activity of the PT – Cu and PT - Zn implants. In general, implants with NPs, as well as the combinations, demonstrated comparable antibacterial leaching activities, however, enhanced compared to the NT, PT, PT - Cu and PT - Zn implants.

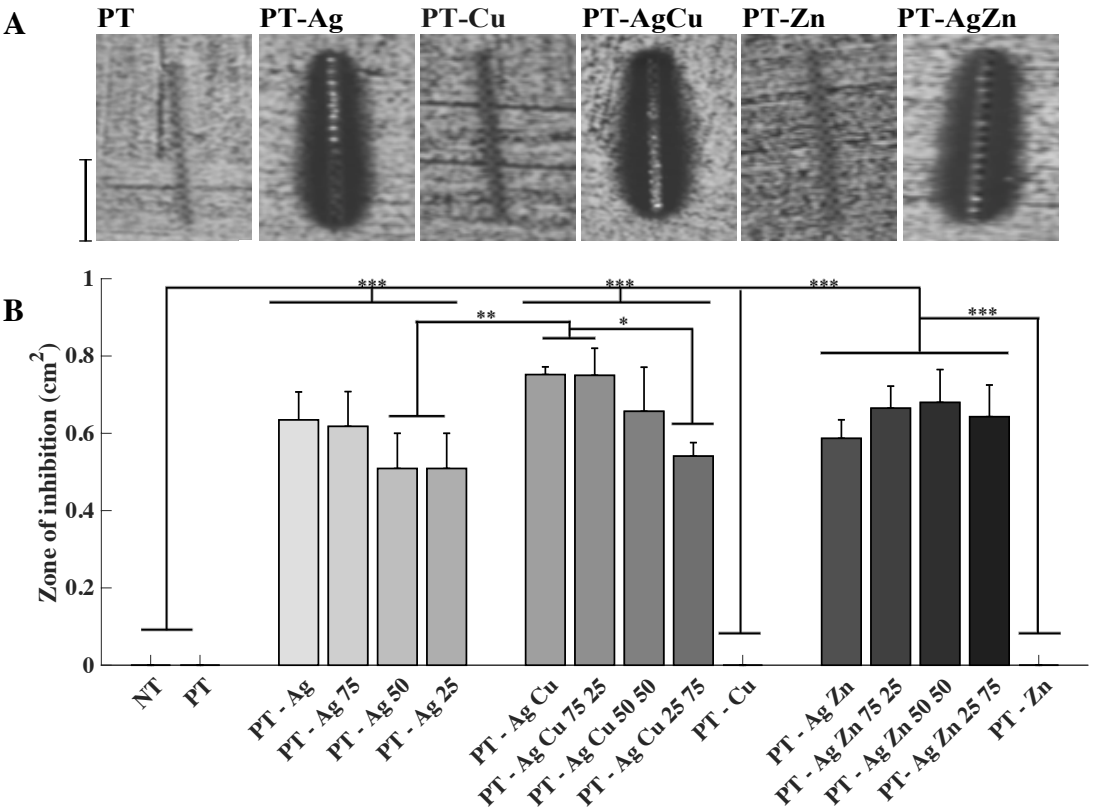

Fig. 11. *In vitro* leachable antibacterial activity of the implants assessed using a modified agar diffusion assay. (A) Photographic images showed inhibition zones around the implants after 24 h of incubation. Scale bar 0.5 cm. (B) Errors bars of the mean surface areas of inhibition zones in cm^2. The surface areas of the inhibition zones were statistically compared between the experimental groups (n = 3/group; *, $p < 0.05$; **, $p < 0.01$; ***, $p < 0.001$).

3.2.1.2 Minimum inhibitory and bactericidal concentration of the ions

To assess the susceptibility of MRSA to Ag^{+}, Cu^{2+} and Zn^{2+} ions, the MIC and MBC for $AgNO_3$, $Cu(NO_3)_2$ and $Zn(NO_3)_2$ were determined using a micro-dilution assay (Fig. 12). After 24 h of incubation, the results indicated that Ag^{+}, Cu^{2+} and Zn^{2+} ions were growth inhibitory and bactericidal to MRSA. The MIC for $AgNO_3$, $Cu(NO_3)_2$ and $Zn(NO_3)_2$ were 0.004 mM, 5 mM and 0.63 mM, respectively. The MBC for $AgNO_3$, $Cu(NO_3)_2$ and $Zn(NO_3)_2$ were 0.06 mM, 10 mM and 5 mM, respectively.

The combinations of Ag^{+} ions with Cu^{2+} and Zn^{2+} ions demonstrated synergism. Lower concentrations of both ions were required to provide inhibitory and bactericidal activities against MRSA. For the combination of Ag^{+} and Cu^{2+}, 0.002 mM of $AgNO_3$ with 5 mM of $Cu(NO_3)$ was required to provide an inhibitory effect. In combination with Zn^{2+} a minimum concentration of 0.31 mM of $Zn(NO_3)_2$ was required with 0.002 mM of $AgNO_3$. In addition, the MBCs of the combinations ranged from 0.03 - 0.002 mM of $AgNO_3$ and either 1.25 - 5 mM of $Cu(NO_3)_2$ or 0.16 - 2.5 mM of $Zn(NO_3)_2$. In short, Ag^{+}, Cu^{2+} and Zn^{2+} ions, as well the combinations of the ions were growth inhibitory and bactericidal to MRSA.

3.2.1.3 Bactericidal activity against surface-adherent and non-adherent MRSA

The bactericidal properties of the implants against MRSA were determined by quantifying the surface-adherent and non-adherent bacteria after 24 h of culture. After the 24 h incubation period, the PT - Ag, PT - Ag 75, PT – Ag 50, PT - Ag Cu, PT - Ag Cu 75 25, PT - Ag Zn and PT - Ag Zn 75 25 implants fully eradicated adherent and non-adherent MRSA. While the PT – Ag 25, PT – Ag Cu 50 50, PT – Ag Cu 25 75, PT – Ag Zn 50 50, PT – Ag Zn 25 75 implants caused a 1-2 log reduction in numbers of surface-adherent and non-adherent MRSA, as compared to the NT, PT, PT – Cu and PT – Zn implants. Significance was only demonstrated for the reduction in numbers of surface-adherent MRSA on the surface of implants with Ag NPs and Zn NPs, as compared with PT - Zn implants ($p < 0.001$). One of the three PT - Ag 25 and PT - Ag Zn 50 50 implants was completely negative in the culture against surface-adherent and non-adherent MRSA. None of the other implants were cultured negatively (Fig. 13).

The results illustrated that substitution of the content of Ag NPs partly with Cu NPs or Zn NPs negatively affected the bactericidal properties. In short, implants with ≥ 50% of Ag NPs and combinations of ≥ 75% of Ag NPs with Cu NPs and Zn NPs, prevented the adhesion of MRSA on the surface of the implants and reduced the number of viable non-adherent MRSA.

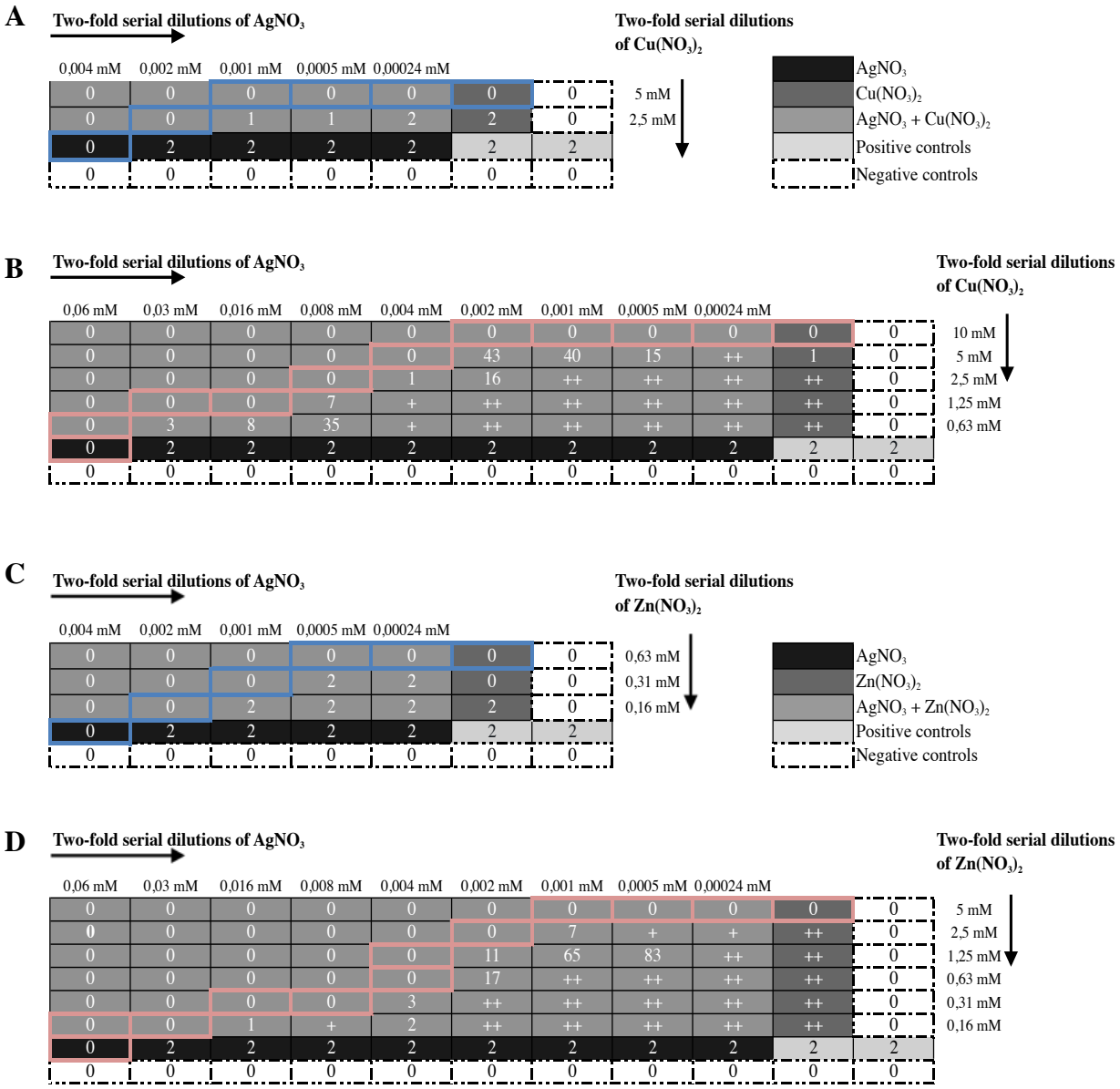

Fig. 12. MIC and MBC of Ag^{+}, Cu^{2+} and Zn^{2+} ions, as well the combinations, against MRSA USA300 determined by a micro-dilution assay. (A) MIC for $AgNO_3$, $Cu(NO_3)_2$, and the combinations. Visual turbidity indicated by 1 and 2. No visual turbidity indicated by 0. (B) MBC for $AgNO_3$, $Cu(NO_3)_2$, and the combinations. Counts of CFUs presented. No CFUs indicated by 0, >100 CFUs indicated by +, countless CFUs indicated by ++. (C) MIC for $AgNO_3$, $Zn(NO_3)_2$, and the combinations. (D) MBC for $AgNO_3$, $Zn(NO_3)_2$, and the combinations.

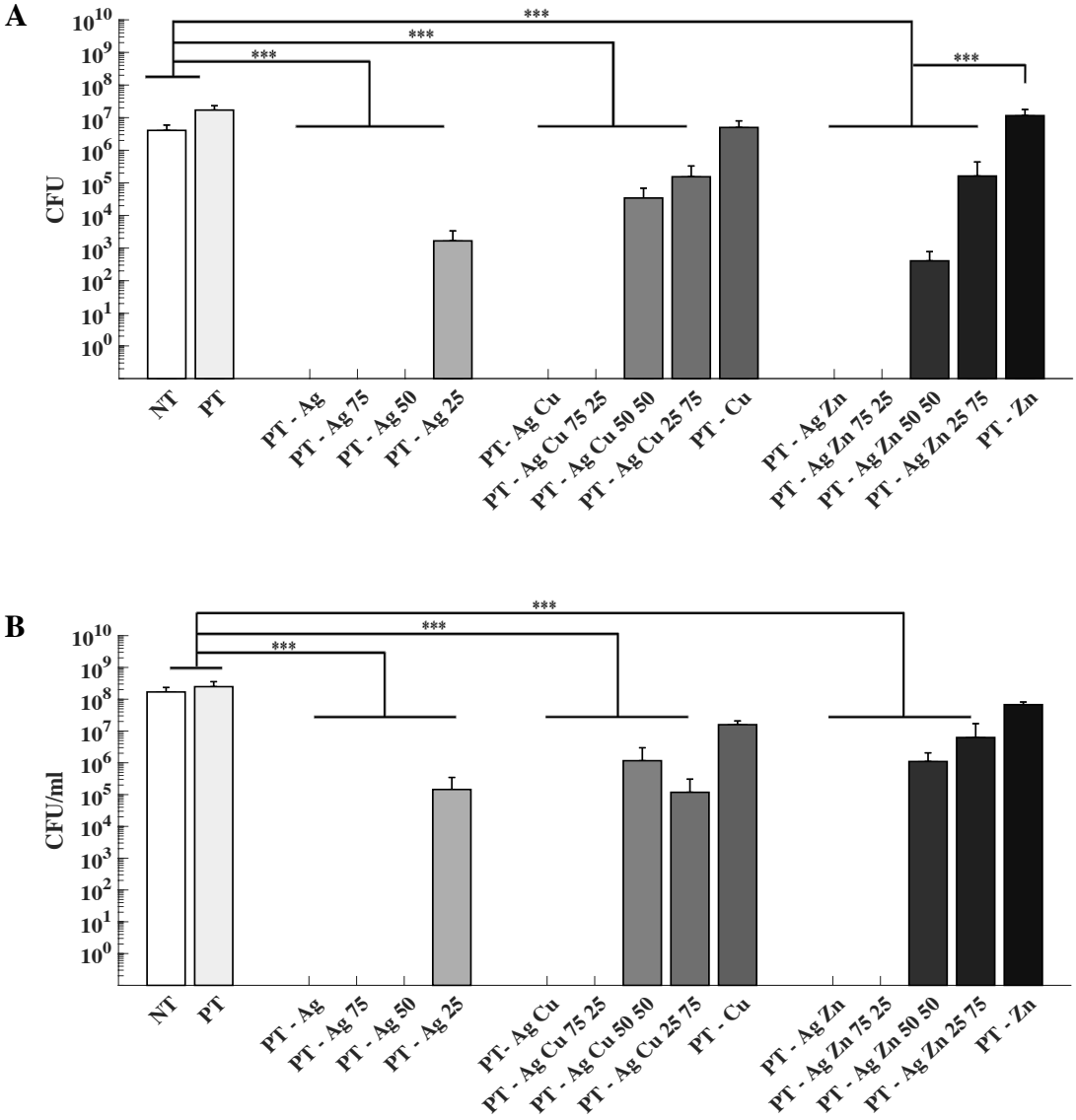

Fig. 13. Bactericidal properties of the implants against surface-adherent and non-adherent MRSA. Four implants were inoculated with 2 x 10^2 CFU of MRSA USA300 and after 24 h of incubation sonicated, collected and quantitatively cultured. MRSA CFU counts of the implants were statistically compared between the experimental groups. (A) CFU quantification of sonicates, reflecting surface-adherent MRSA. (B) CFU quantification of TSB culture medium, reflecting non-adherent MRSA (n = 3/group; ***, $p < 0.001$).

3.2.1.4 Anti-biofilm activity

Anti-biofilm properties of the implants were investigated by culturing the implants for 24 h with MRSA under conditions that induced biofilm formation and consequently analyzed using SEM. After 24 h of incubation, bacterial adhesion was demonstrated on significant parts of the surface of NT (Fig. 14A), PT (Fig. 14B), PT - Ag 25 (Fig. 15B), PT - Ag Cu 5050 (Fig. 16A), PT - Ag Cu 25 75 (Fig. 16B), PT - Cu (Fig. 16C), PT - Ag Zn 50 50 (Fig. 17B), PT - Ag Zn 25 75 (Fig. 17C) and PT - Zn implants (Fig. 17D). Clusters of bacterial cells ranging from a few dozen to hundreds of bacterial cells, grown up to 2 - 4 layers, were observed on the surface of the implants. In addition, signs of biofilm formation were demonstrated for the NT implant. No biofilm formation signs were observed for the other implants.

Significantly reduced numbers of surface-adherent bacteria were detected on the surface of PT – Ag (Fig. 14C), PT - Ag 75 (Fig. 14D), PT - Ag 50 (Fig. 15A), PT - Ag Cu (Fig. 15C), PT – Ag Cu 75 25 (Fig. 15D), PT - Ag Zn (Fig. 16D) and PT - Ag Zn 75 25 implants (Fig. 17A). A few clusters of bacterial cells attached in the deep micro-pores of the biofunctionalized TiO_2 surface layers were demonstrated. In addition, a decreased cluster size was observed, varying from a single to ten bacterial cells. The results demonstrated that substitution of the content of Ag NPs partly with Cu NPs or Zn NPs negatively affected the anti-biofilm properties. In short, implants with $\geq$ 50% of Ag NPs and combinations of $\geq$ 75% of Ag NPs with Cu NPs and Zn NPs, prevented biofilm formation up to 24 h.

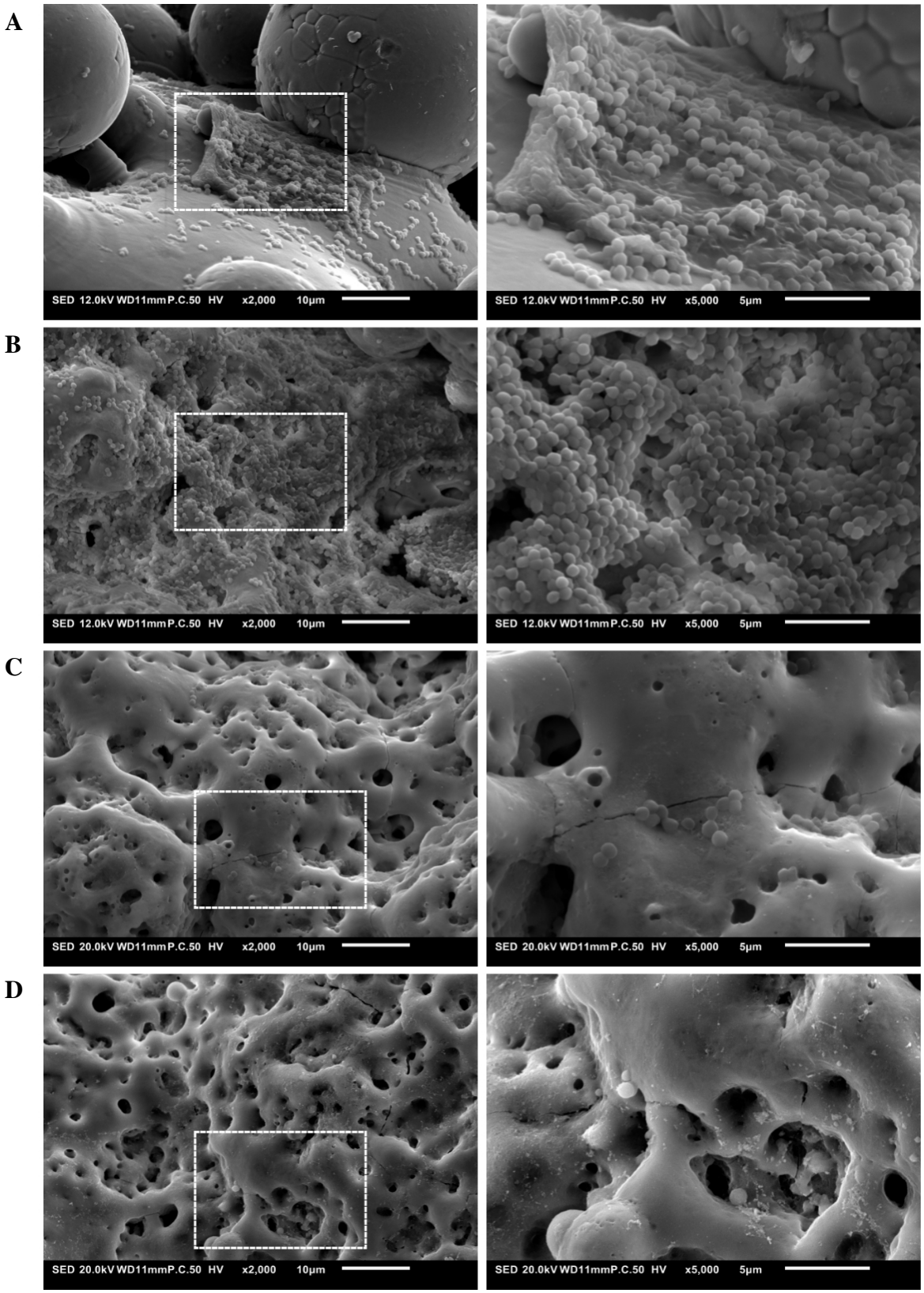

Fig. 14. Low (2000x) and high (5000x) magnification SEM images of MRSA USA300 biofilm formation on the surface of the implants after 24 h of incubation with 2 x 10^2 CFU of MRSA. (A) NT. (B) PT. (C) PT – Ag. (D) PT – Ag 75 implants.

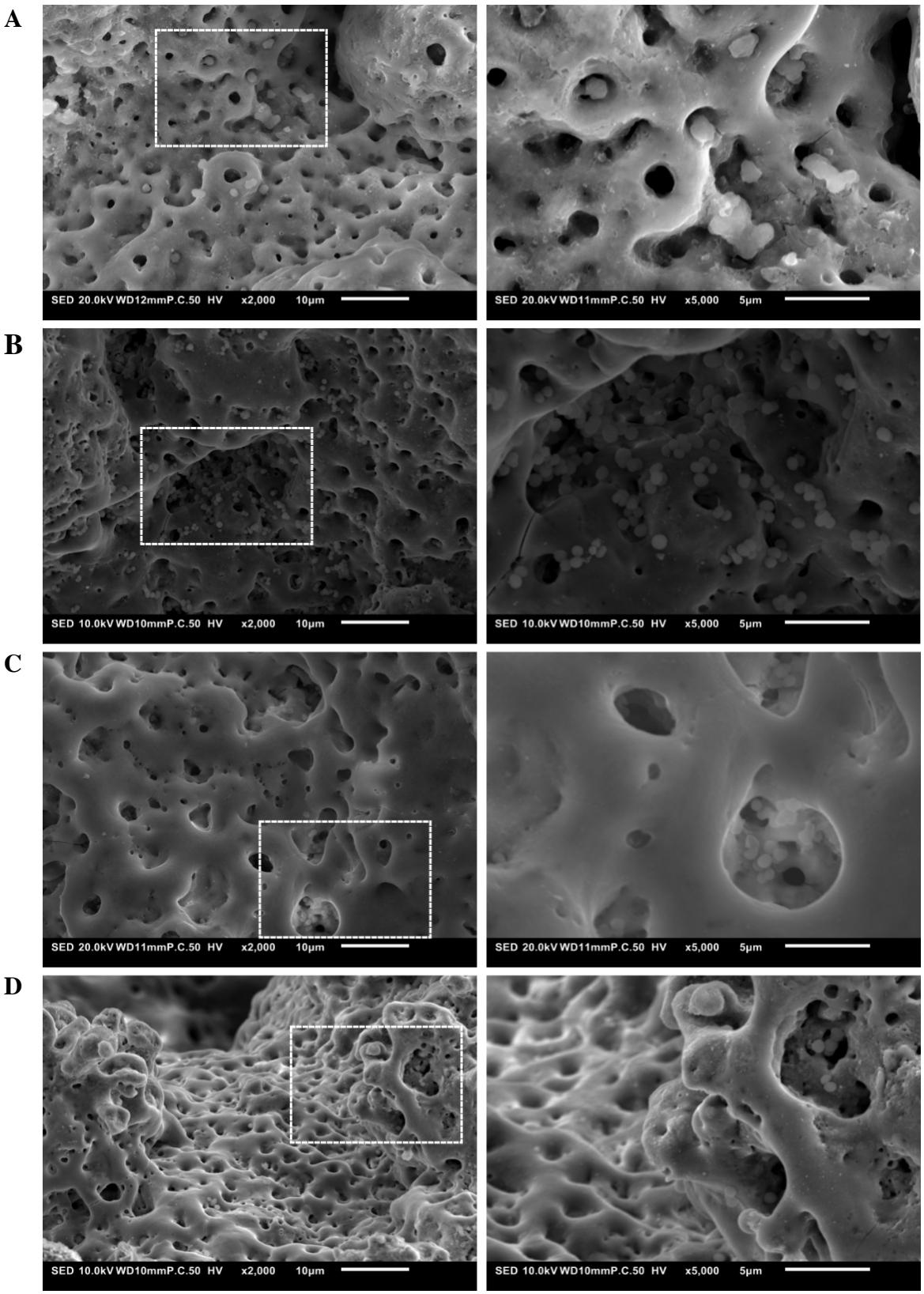

Fig. 15. Low (2000x) and high (5000x) magnification SEM images of MRSA USA300 biofilm formation on the surface of the implants after 24 h of incubation with 2 x 10^2 CFU of MRSA. (A) PT – Ag 50. (B). PT – Ag 25. (C) PT – Ag Cu. (D) PT – Ag Cu 75 25 implants.

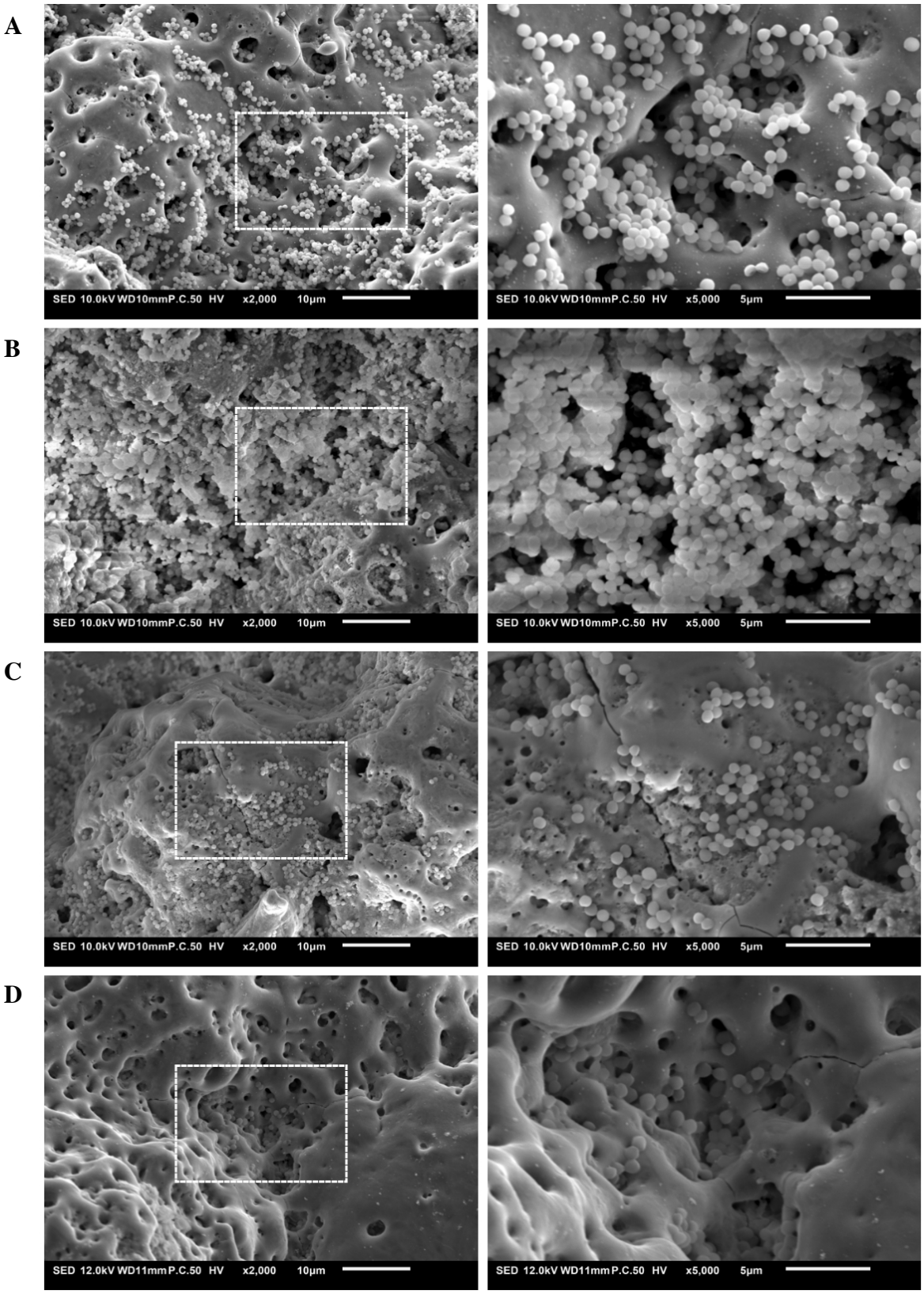

Fig. 16. Low (2000x) and high (5000x) magnification SEM images of MRSA USA300 biofilm formation on the surface of the implants after 24 h of incubation with 2 x 10^2 CFU of MRSA. (A) PT – Ag Cu 50 50, (B) PT – Ag Cu 25 75. (C) PT – Cu. (D) PT – Ag Zn implants.

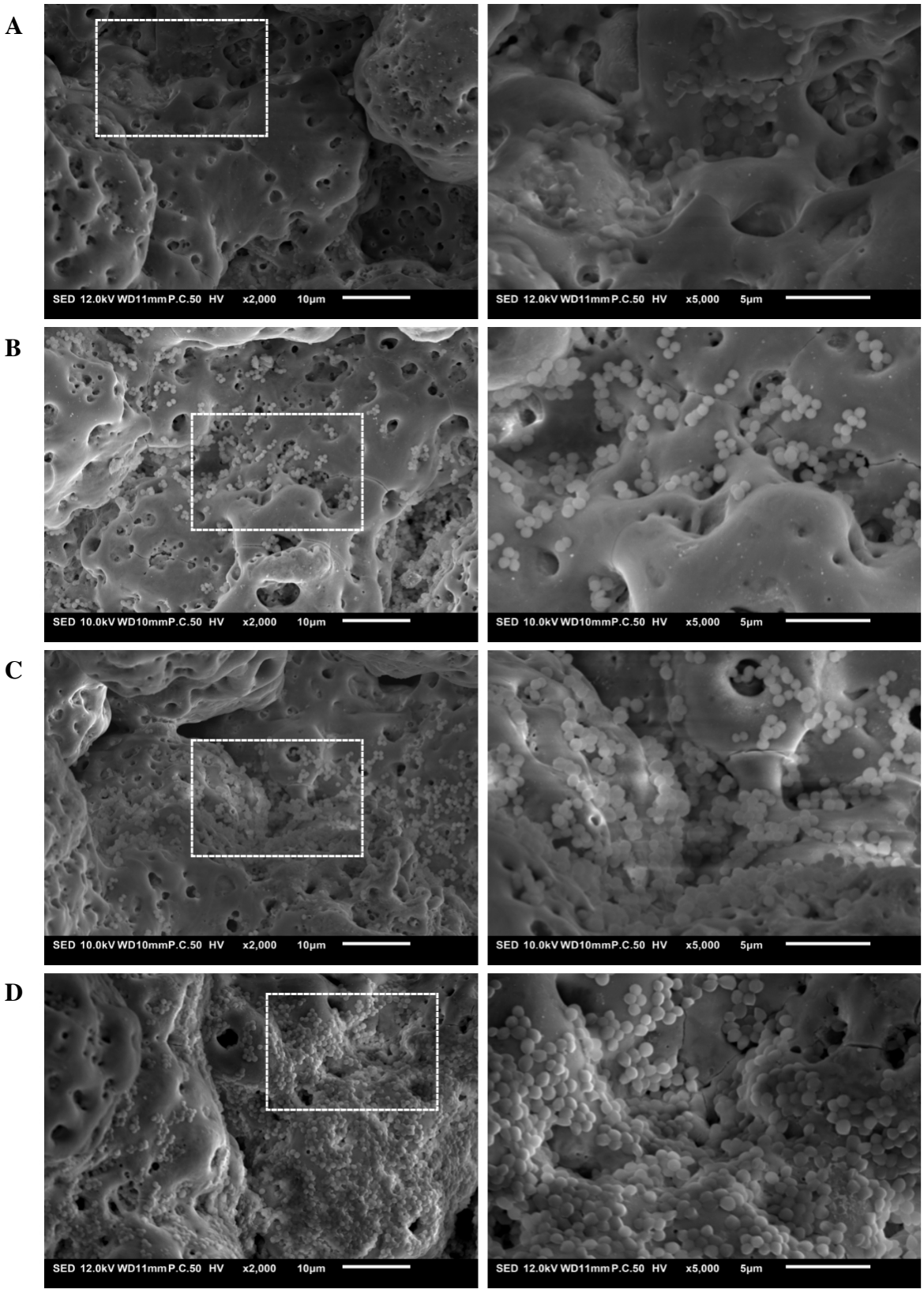

Fig. 17. Low (2000x) and high (5000x) magnification SEM images of MRSA USA300 biofilm formation on the surface of the implants after 24 h of incubation with 2 x 10^2 CFU of MRSA (A) PT – Ag Zn 75 25. (B) PT – Ag Zn 50 50. (C) PT – Ag Zn 25 75. (D) PT – Zn implants.

3.2.2 *Ex vivo* antibacterial activity of the implants

To investigate the *ex vivo* antibacterial properties of the implants against MRSA, a femoral murine infection model was used that mimicked the *in vivo* environment. After the 24 h incubation period, the PT - Ag, PT - Ag Cu, PT - Ag Cu 75 25, PT - Ag Zn and PT - Ag Zn 75 25 implants fully eradicated MRSA in the femoral murine infection model, while PT – Ag 50 implants caused a 2-3 log reduction in numbers of MRSA, as compared to NT and PT implants (Fig. 18).

In short, implants with ≥ 50% of Ag NPs and combinations of ≥ 75% of Ag NPs with Cu NPs and Zn NPs, limited bacterial growth in a *ex vivo* femoral murine infection model, as compared to NT and PT implants.

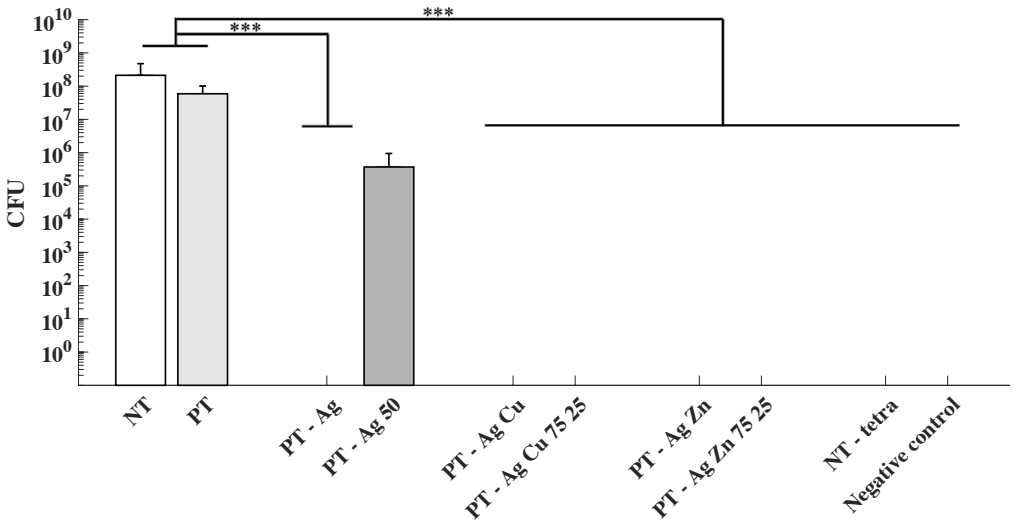

Fig. 18. *Ex vivo* antibacterial activity of the implants against MRSA assessed in a femoral murine infection model. Implants were inoculated with 2 x 10^2 CFU of MRSA USA, implanted into the mouse femurs and after overnight incubation, homogenized and quantitatively cultured. MRSA CFU counts of the implants were statistically compared between the experimental groups. The *ex vivo* model was valid, as evidenced by the NT - tetra (injected with tetracycline hydrochloride) and negative control (no implant received). No bacterial growth was observed (n = 3/group; ***, $p < 0.001$).

4 Discussion

AM techniques are capable of manufacturing porous biomaterials that have shown to improve bone tissue integration and regeneration. AM porous implants, however, are at enhanced risks of IAIs. Hence, these porous implants require integrated antibacterial properties. The current study aimed to evaluate and systematically compare the antibacterial properties of AM porous Ti6Al4V implant surfaces with Ag NPs, Cu NPs and/or Zn NPs against MRSA, synthesized by a one-step PEO process. The results of the current study demonstrated strong *in vitro* as well as *ex vivo* antibacterial properties of the porous implants with Ag NPs and Cu NPs or Zn NPs. Implants with ≥ 50% of Ag NPs and combinations of ≥ 75% of Ag NPs and Cu NPs or Zn NPs, fully eradicated surface-adherent and non-adherent MRSA within 24 h and prevented MRSA biofilm formation *in vitro* up to 24 h, one of the most virulent pathogens that cause IAIs. Moreover *ex vivo* bactericidal properties against MRSA were demonstrated for these implants. No synergism was observed on the antibacterial properties.

4.1 Discussion of results

In the current study, porous Ti6Al4V implants were additively manufactured using SLM and subsequently biofunctionalized by PEO, to synthesize a firmly adherent TiO_2 surface layer that incorporated various ratios of Ag NPs, Cu NPs and/or Zn NPs. The parameters of the PEO process used in the current study (300 sec, 20 A/dm^2) resulted in micro-/nano-porous morphologies with well-separated interconnected pores, varying in size from a couple of nm to 5 μm, at the outer sections of the TiO_2 surface layer (Fig. 8). Incorporation of various ratios of Ag NPs, Cu NPs and/or Zn NPs in the TiO_2 surface layers by PEO did not alter the morphological characteristics of the oxide layers. In addition, similar chemical compositions were demonstrated for the oxide layers, irrespectively of the ratios of NPs incorporated (Fig. 10). As a result, the effect of various ratios of NPs on the antibacterial properties of the implants could be evaluated in the current study, without the intercession of the former factors [66,67]. Preclinical studies demonstrated that the biological performances of Ti-based surfaces, such as antibacterial and osteogenic properties, were influenced by the surface properties, including surface topography chemistry, of Ti and its alloys [52,68]. Moreover, the resulting surface characteristics, including morphology, pore size and chemical composition, were in accordance with previous studies on PEO processing of Ti alloys using similar electrolytes [60,69], reflecting the suitability of the one-step PEO process for AM porous implants.

The incorporation of Ag NPs and Cu NPs or Zn NPs, in the implant surface has resulted in multifaceted antibacterial properties against MRSA. The leaching activity of the implants with Ag NPs and Cu NPs or Zn NPs caused a clear growth inhibition zone of MRSA, while no growth inhibition zones were observed around the implants without Ag NPs (Fig. 11). These results coincide with the released Ag^+, Cu^{2+} and Zn^{2+} ion concentrations, reported in previous studies [62,65] and the obtained MIC of the ions (Fig. 11).

The reported maximal cumulative Cu^{2+} and Zn^{2+} ion release concentrations of 1 ppm and 0.86 ppm from the implants within 24 h, respectively, were far below the MIC of these ions, i.e. 5 mM and 0.63 mM (equivalent to a Cu^{2+} and Zn^{2+} ion concentration of 317.73 and 41.20 ppm) [62,65]. As a result, the exhibited antibacterial leaching activity of the implants was caused by the released Ag^{+} ions from the Ag NPs in the TiO_2 surface layer. This assumption correlated with reported cumulative Ag^{+} ion release concentration within 24 h, i.e. 0.86 ppm, which is higher than the MIC of Ag^{+} ions, i.e. 0.04 mM (equal to an Ag^{+} ion concentration of 0.43 ppm) [62,65]. Superiority of the Ag^{+} ions was hence demonstrated in comparison with the Cu^{2+} and Zn^{2+} ions [9]. The design of the agar diffusion assay used in the current study did, however, not elucidate whether the antibacterial leaching activity of the implants was bactericidal to MRSA. Bactericidal leaching activity in the peri-implant area is, nevertheless, required to prevent infection of peri-implant area, since the peri-implant area forms a niche for bacterial colonization [70,71].

Bactericidal activities of the implants against planktonic (i.e. non-adherent) bacteria have been demonstrated in the current study (Fig. 13B). The quantitative CFU count assay showed that the PT - Ag, PT - Ag 75, PT - Ag 50, PT - Ag Cu, PT - Ag Cu 75 25, PT - Ag Zn and PT - Ag Zn 75 25 implants not only inhibited MRSA growth around the implants, but completely killed them as well. These results highlight the significantly higher antibacterial functionality of Ag NPs compared to Cu NPs and Zn NPs, as shown by a 1000-times increase in numbers of MRSA for the PT - Cu and PT - Zn implants. The observed antibacterial properties may, however, not be fully attributed to the released ions from the NPs, as the released Ag^{+} ion concentration within 24 h was lower than the reported MBC of 0.06 mM (equal to an Ag^{+} ion concentration of 6.4 ppm) [65]. Possible factors that might contribute to the bactericidal activity of the implants are the secondary products generated by the NPs and ions, such as ROS [72-75]. Reportedly, ROS can enter the bacterial cell envelope and damages the deoxyribonucleic acid (DNA), resulting in bacterial apoptosis i.e. cell death [76,77]. Besides that, a pioneering study recently showed crystalline anatase and rutile phases in the TiO_2 surface layer of AM porous implants, which causes ROS generation [60,78]. Hence, a multifaceted antibacterial mechanism can be proposed. However, to confirm this assumption, the amounts of ROS generated by the TiO_2 surface layer, the NPs and the ions and their role in the observed antibacterial properties must be verified.

Besides that, it is of importance to note that the PT - Ag 50 implants fully eradicated MRSA, while PT - Ag Cu 50 50 and PT-Ag Cu 50 50 implants repressed bacterial growth with 1 - 2 logs, compared to implants without Ag NPs. These results indicated that adding ≥ 50% of Cu NPs and Zn NPs to Ag NPs negatively affected the bactericidal properties of the implants. This is in contrast to the presented MIC and MBC results (Fig. 11) and previously reported work [79,80]. Recently it has been shown that the combinations of Ag^{+} ions with Cu^{2+} and Zn^{2+} ions demonstrated synergism on the antibacterial properties. Lower concentrations of each antibacterial agent were required to provide inhibitory and bactericidal activities against MRSA. The released Cu^{2+} and Zn^{2+} ion concentrations from the implants used in the current study were, however, not sufficient to exert an inhibitory effect against MRSA, as previously have been demonstrated. As consequence, no synergism has been demonstrated in the current study.

The results presented might, however, be associated with the occurrence of micro-galvanic couplings between Ag NPs, Cu NPs and Zn NPs, which has been shown to alter the release kinetics of the antibacterial agents [80,81]. Recently it became evident that simultaneous incorporation of Ag and Zn in titanium resulted in micro-galvanic couplings after immersion in a physiological saline solution, which caused a preferred Zn^{2+} ion release, while preserving the Ag NPs on the titanium surface i.e. reduced Ag^{+} ion release [80]. In the current study, however, the released Ag^{+} ion has shown to largely provoke the antibacterial functionality, while the released Cu^{2+} ion and Zn^{2+} ion concentrations from the NPs were not sufficient to pose any antibacterial effect against MRSA. Hence, it is reasonable to assume that the released Cu^{2+} ion and the Zn^{2+} ion concentrations from the PT - Ag Cu 50 50 and PT - Ag Zn 50 50 implants in the presented study were unable to substitute the reduced released Ag^{+} ion concentration, which adversely affected the antibacterial functionality of the implants.

In addition, the results may be related to the amount of antibacterial agent incorporated in the TiO_2 surface layer. It has recently been shown that simultaneous incorporation of Ag and Zn in titanium through ion implantation resulted in a reduced surface content of both antibacterial agents, compared to single-ion implanted Ag and Zn titanium [80]. Additionally, simultaneous incorporation of Cu and Zn in titanium by PEO, recently showed a reduction in the surface content of Cu, compared to PEO biofunctionalized titanium with only Cu [82]. In concert with these results, it is reasonable to assume that PT - Ag Cu 50 50 and PT - Ag Zn 50 50 implants contained a lower surface content of Ag NPs, compared to PT - Ag 50 implants, due to the addition of Cu NPs and Zn NPs. Moreover, the antibacterial properties of the implant have proved to be dependent on the amount of antibacterial agent incorporated in the surface layer [83-85]. These results suggest that a reduced surface content adversely affects the antibacterial properties, in accordance with the results presented in this study. The surface content of NPs in the TiO_2 surface layer must, however, be quantified to confirm this assumption [86].

Nevertheless, the current study indicated that Cu^{2+} and Zn^{2+} ions were growth inhibiting and bactericidal for MRSA (Fig. 11), in concert with previous studies [87,88]. Enhanced Cu NPs and Zn NPs contents should hence be incorporated in the implant surface to pose antibacterial effects against MRSA and to benefit from the micro-galvanic couplings, as recently illustrated [86-88].

Moreover, prevention of bacterial adhesion is critical to preclude biofilm formation on the surface of the implant [89]. The implants with $\geq$ 50% of Ag NPs and combinations of $\geq$ 75% of Ag NPs and Cu NPs or Zn NPs showed to fully eradicate surface-adherent MRSA within 24 h (Fig. 13A) and prevented *in vitro* MRSA biofilm formation up to 24 h (Fig. 14-17), with only a few MRSA clusters attached in the deep micro-pores. A 1000-times increase in numbers of surface-adherent MRSA were, however, reported for implants without Ag NPs (Fig. 13A). These results were in accordance with the SEM images of MRSA biofilm formation (Fig. 14-15). The *in vitro* setup of the biofilm formation assay in the current study did, however, not elucidate whether the few dozen of MRSA attached to the implant surface were viable. Viable MRSA, although in a small number, pose risks for biofilm formation and initiation of IAIs [74,89].

Furthermore, an *ex vivo* bactericidal effect after 24 h of the implants with NPs was illustrated in a femoral murine infection model mimicking the *in vivo* environment. Bactericidal properties were induced by the implants with ≥ 50% of Ag NPs and combinations of ≥ 75% of Ag NPs and Cu NPs or Zn NPs, while no bactericidal properties were shown for the NT and PT implants (Fig. 18). These results are in accordance with the other antibacterial results presented in the current study. It is worth noting that the *ex vivo* infection model could not benefit from an active immune system that could further reduce the numbers of MRSA [90]. This observation therefore suggests a potential for the *in vivo* bactericidal activity of the implants with Ag NPs. In addition, the suitability for *in vivo* application was demonstrated, since the infected biomaterial was successfully implanted at the intended site of application [7]. However, it is of importance to note that due to the design of the *ex vivo* assay, it is not clear whether the viable numbers of MRSA adhered to the surface of the implants or migrated to the peri-implant area (i.e. bone tissue).

In general, the results of the present study consistently showed enhanced antibacterial properties of implants with Ag NPs, singular and in combination with Cu NPs and Zn NPs, than implants without Ag NPs. The antibacterial properties of the implants are due to the Ag NPs present in the surface. In combination with Cu NPs and Zn NPs, ≥ 75% of Ag NPs was required to achieve strong antibacterial properties, while ≥ 50% of Ag NPs was required without Cu NPs or Zn NPs additions.

4.2 Significance and recommendations

AM porous implants require integrated antibacterial properties. Pioneering research has recently demonstrated strong antibacterial properties *in vitro* and *ex vivo* against MRSA for porous AM Ti6Al4V implants with Ag NPs, synthesized by a one-step PEO process [60]. Preliminary results have shown that AM titanium implants with Ag NPs and Cu NPs or Zn NPs could be synthesized by PEO [62,65]. However, in the current literature there is no systematic comparison of the antibacterial properties of Ti-based surfaces with Ag NPs, Cu NPs and/or Zn NPs available [91]. The current study therefore provided a systematic comparison of the antibacterial properties of AM porous Ti6Al4V implant surfaces with Ag NPs, Cu NPs and/or Zn NPs against MRSA, synthesized by PEO process. Hence, the current study is the first study to provide a systematic comparison of the effects of various ratios of NPs incorporated in the surface, without the intercession of factors [9,12].

Overall, the implants manufactured in the current study may have the potential to prevent IAIs [7]. Implants with ≥ 50% of Ag NPs and combinations of ≥ 75% of Ag NPs and Cu NPs or Zn NPs demonstrated multifaceted antibacterial properties against MRSA after 24 h, including leachable antibacterial activity, bactericidal properties against surface-adherent and non-adherent MRSA and prevention of biofilm formation. Moreover, *ex vivo* bactericidal properties against MRSA were demonstrated for these implants. Nevertheless, further research is required to explore the suitability of these implants for clinical applications.

Reportedly, Ag NPs, Cu NPs and Zn NPs tend to provide antibacterial properties against numerous Gram-negative and Gram-positive bacteria [22-24]. However, to strengthen the protective capabilities demonstrated in the present study, the antibacterial properties of the implants must be tested against other *Staphylococci* strains, such as *S. epidermis* [92]. Recently it was reported that different bacterial species show varying virulence and susceptibility to antibacterial agents [93]. In addition, *Staphylococci* strains, which account for more than 50% of IAI cases, have developed resistance to conventional antibiotics, limiting their clinical effectiveness [20,92]. Effective preventive measures must hence require antibacterial properties against various pathogenic *Staphylococci* strains, including antibiotic-resistant strains.

In addition, effective preventive measures must be simultaneously aimed at the prevention of perioperative infections (i.e. immediately after implantation [7]) as well as late, or haematogenous infections [94]. The presented results, demonstrated the potential to prevent perioperative infections, because the implants with NPs provided bactericidal properties against free-living bacteria within 24 h and prevented MRSA biofilm formation up to 24 h. The long-lasting antibacterial properties were, however, unexplored in the current study. Pioneering research, nevertheless, demonstrated long-lasting antibacterial properties *in vitro* and *in vivo* against MRSA for titanium with Ag NPs up to 30 days [95]. Future research should therefore have the emphasis on long-term testing of the antibacterial properties of the implants manufactured in the current study.

Furthermore, it is, nevertheless, of importance to note that the current study indicated that adding ≥ 50% of Cu NPs and Zn NPs to Ag NPs negatively affected the bactericidal properties of the implants. Factors possibly contributing were ascribed to the surface content of Ag NPs in the TiO_2 surface layer and the occurrence of micro-galvanic couplings between Ag NPs, Cu NPs and Zn NPs. In the current study, the surface content of Ag NPs, Cu NPs and Zn NPs in the TiO_2 surface layer is unexplored. The surface content of NPs in the TiO_2 surface layer should be quantified by dissolving the TiO_2 surface layer in sulfuric acid and quantifying the ion concentrations with inductively coupled plasma-mass spectrometry technique (ICP-MS) [86]. To verify the occurrence of micro-galvanic couplings on the implant surface, the corrosion potential of the implants with Ag NPs and Cu NPs and Zn NPs should be measured [80-81].

Moreover, the design of the agar diffusion assay used in the current study did not elucidate whether the antibacterial leaching activity of the implants was bactericidal to MRSA, as mentioned above. Cultures from the inhibition zones are hence required to verify whether the released ions from the NPs fully eradicated MRSA, as demonstrated in a previous study [60]. In addition, the *in vitro* setup of the anti-biofilm activity assay did not elucidate whether the surface-adherent MRSA on the implants surface, revealed by SEM, are viable and capable of proliferating on the surface of the implant. Previous studies used a Live/Dead fluorescence-staining assay to quantify the surface-adherent bacterial cell viability on the implants surface after a period of culture [83,96]. Further research should therefore involve a Live/Dead fluorescence-staining assay in combination with biofilm formation SEM images, to assess the anti-biofilm activity of the implants.

Nonetheless, it is important to recap that the released Cu^{2+} and Zn^{2+} ion concentrations from the implants used in the current study were not sufficient to exert an inhibitory effect against MRSA. As a result, no synergy has been demonstrated. Enhanced Cu NPs and Zn NPs contents should hence be incorporated in the implant surface, to induce bactericidal activities. Recently it has, however, been stated that the mean half maximal inhibitory concentration (IC_{50}) of Zn^{2+} ions of osteoblasts viability is 0.09 mM (equivalent to a Zn^{2+} ion concentration of 12.26 ppm) [97], which is much lower than the MIC of Zn^{2+} ions required, to pose any antibacterial effect against MRSA. The potential cytotoxicity makes it hence prudent to concentrate in further research on the implants with NPs, which minimizes cytotoxicity and maintains antibacterial effectiveness [30].

In the current study no cytotoxicity assays have, however, been conducted, to evaluate the cytotoxic effects of the implants on osteogenic cells e.g. MSCs. Nevertheless, the maximal cumulative Ag^{+}, Cu^{2+} and Zn^{2+} ion release concentrations of 1.91 ppm, 2.51 ppm and 2.28 ppm from the implants over 28 days, were far below the IC_{50} value of these ions of osteoblasts viability (≈ 10 ppm, 10 ppm and 12.26 ppm, respectively) [97-99], suggesting that the implants manufactured in the current study may be biocompatible. In addition, the implants might potentially improve the bone tissue regeneration performance and implant integration, particularly the implants with Cu NPs and Zn NPs. Pioneering research has shown that porous AM titanium implant surface with Ag NPs synthesized by PEO, supported cellular functions of human MSCs, due to the developed micro-/nano-porous surface morphology and the presence of Ca/P-based elements in the surface [60]. It has been shown that the typical PEO morphology and Ca/P-based surface chemistry, stimulated the implant bone tissue regeneration and integration, compared to implants without biofunctionalization [100,101]. The results presented, demonstrated the presence of a uniform and homogeneous micro-/nano-porous oxide layer covering the entire implant surface and containing Ca/P-based elements. In addition, previous studies have shown stimulated implant bone tissue regeneration and integration performance, as a result of the incorporation of Cu and Zn elements in the surface [30,102]. In addition, the implants should not compromise the immune competence of the local host i.e. cytotoxic effects on the immune cells [7]. Further research should hence investigate the *in vitro* cytotoxicity/bioactivity of the implants with ≥ 50% of Ag NPs and combinations of ≥ 75% of Ag NPs and Cu NPs or Zn NPs on human MSCs and immune cells.

Moreover, the presented study studied the antibacterial properties in monoculture models i.e. in the presence of only bacterial cells. Further research should, however, include *in vitro* co-culture models that use eukaryotic cells (i.e. human MSCs and immune cells) and bacterial cells, to examine the host-pathogen cell interaction on the implant resembling the *vivo* environment [103,104]. Apart from that, the suitability of the implants for *in vivo* application was in the current study demonstrated using an *ex vivo* femoral murine infection model. The infected biomaterial was successfully implanted at the intended site of application and provided strong antibacterial properties *ex vivo* [7,90]. Further research should therefore proceed to *in vivo,* to assess the performance of the implants in a complete biomimetic environment.

5 Conclusion

To address IAIs and implant longevity simultaneously, medical grade porous Ti6Al4V implants were additively manufactured using SLM and subsequently biofunctionalized by PEO, to incorporate various ratios of Ag NPs, Cu NPs and/or Zn NPs in the micro-/nano-porous oxide surface layer. Biomaterial characteristics and *in vitro* as well as *ex vivo* antibacterial properties of the manufactured implants were evaluated and systematically compared. Biomaterial characterization revealed that, the morphological characteristics and chemical compositions of the surface of the implants were comparable. Strong antibacterial properties of the implants with Ag NPs and Cu NPs or Zn NPs against MRSA were consistently demonstrated, including leachable antibacterial activity, bactericidal properties against surface-adherent and non-adherent MRSA and prevention of biofilm formation. Moreover, *ex vivo* bactericidal properties against MRSA were demonstrated for these implants. No antibacterial properties were observed for the implants without Ag NPs. The antibacterial properties of implants with NPs are due to the Ag NPs present in the surface. In combination with Cu NPs and Zn NPs, ≥ 75% of Ag NPs were required to achieve bactericidal properties, while ≥ 50% of Ag NPs were required without Cu NPs or Zn NPs additions. No synergism was hence demonstrated on the antibacterial properties. Based on these findings, the implants with 50% of Ag NPs and combinations of 75% of Ag NPs and 25% of Cu NPs or Zn NPs could be considered as promising for further development, to prevent IAIs and to improve implant longevity in clinical applications.

6 Acknowledgment

''During my thesis I received a lot of support from different people. First of all, I want to thank my daily supervisor Ir. Ingmar A.J van Hengel. Ingmar taught me various experiments during my thesis with great pleasure and enthusiasm. Moreover, his door was always open to me, which resulted in many important discussions with the necessary input. Furthermore, I am very grateful to Dr. Ir. Lidy Fratila-Apachitei for her support and for arranging the cooperation with the UMC Utrecht. I would like to thank her for the input and the advice she gave during innumerable meetings. In addition, I am very grateful to Prof. Dr. Ir. Amir A. Zadpoor for his input and assistance with the realization of the manuscript. I am grateful to them all, because they gave me the opportunity to undertake this interesting master's thesis project at the Department of Biomechanical Engineering at TU Delft.

Moreover, the antibacterial experiments could not be conducted without the excellent cooperation with the Microbiology department at UMC Utrecht, in particular thanks to W.C. De Graaf, B.J Benaissa Trouw and Dr. Ad Fluit. In addition, I would like to thank Ron Timmermans from the UU, for supplying the mouse femurs that were needed to perform the *ex vivo* antibacterial experiments. At last, I want to thank Niko Eka Putra for his support and help at PEO, Raisa Grotenhuis for her help during some antibacterial experiments, Munzur Lacin for his support during my thesis and for his help at SEM and Sander Leeflang for his technical support.''

7 Abbreviations

AM	Additive manufacturing / additively manufactured
CAMH	Cation-Adjusted Mueller Hinton
CFU	Colony-forming unit
DNA	Deoxyribonucleic acid
EDS	Energy dispersive X-ray spectroscopy
IAI	Implant-associated infection
ICP-MS	Inductively coupled plasma-mass spectrometry technique
IC_{50}	Half maximal inhibitory concentration
LB	Luria-Bertani
MBC	Minimum bactericidal concentration
MIC	Minimum inhibitory concentration
MRSA	Methicillin-resistant *Staphylococcus aureus*
MSCs	Mesenchymal stem cells
NPs	Nanoparticles
NT	Non-treated
OD_{600}	Optical density at 600 nm wavelength
PEO	Plasma electrolytic oxidation
PBS	Phosphate-buffered saline
PPM	Parts per million
PT	PEO-treated
ROS	Reactive oxygen species
RPM	Rotations per minute
SEM	Scanning electron microscopy
SLM	Selective laser melting / melted
TiO_2	Titanium oxide
TSB	Tryptic soy broth
TU Delft	Delft University of Technology
UMC	University Medical Center
UU	University Utrecht
V-t	Voltage-time

8 References

[1] Gheno, R., Cepparo, J.M., Rosca, C.E., Cotten, A. (2012). Musculoskeletal Disorders in the Elderly. *Journal of Clinical Imaging Science, 2*, 39.

[2] Salter, R.B. (1989). The biologic concept of continuous passive motion of synovial joints - the 1st 18 years of basic research and its clinical-application. *Clinical Orthopaedics and Related Research, 242,* 12-25.

[3] Hernlund, E., Svedbom, A., Ivergård, M., Compston, J., Cooper, C., Stenmark, J., McCloskey, E.V., Jönsson, B., Kanis, J.A. (2013). Osteoporosis in the European Union: medical management, epidemiology and economic burden. A report prepared in collaboration with the International Osteoporosis Foundation (IOF) and the European Federation of Pharmaceutical Industry Associations (EFPIA). *Archives of Osteoporosis, 8*, 136.

[4] Agarwal, R., & García, A. J. (2015). Biomaterial strategies for engineering implants for enhanced osseointegration and bone repair. *Advanced Drug Delivery Reviews, 94,* 53–62.

[5] Veerachamy, S., Yarlagadda, T., Manivasagam, G., Yarlagadda, P.K. (2014). Bacterial adherence and biofilm formation on medical implants: a review. *Proceedings of the Institution of Mechanical Engineers, Part H: Journal of Engineering in Medicine*, *228*(10), 1083-1099.

[6] Qin, S., Xu, K., Nie, B., Ji, F., Zhang, H. (2018). Approaches based on passive and active antibacterial coating on titanium to achieve antibacterial activity. *Journal of Biomedical Materials Research: Part A, 106*(9), 2531-2539.

[7] Busscher, H.J., Van der Mei, H.C., Subbiahdoss, G. Jutte., P.C., Van den Dungen, J.J.A.M, Zaat, S.A.J., Schultz, M.J., Grainger, D.W. (2012). Biomaterial-associated infection: locating the finish line in the race for the surface. *Science Translation Medicine*, *4*(153), 153rv10.

[8] Costerton, J.W., Stewart, P.S., Greenberg, E. (1999). Bacterial biofilms: a common cause of persistent infections. *Science*, *284*,1318–1322.

[9] Ferraris, S., Spriano, S. (2016). Antibacterial titanium surfaces for medical implants. *Materials Science and Engineering C, 6*1, 965-978.

[10] Kapadia, B.H., Berg, R.A., Daley, J.A., Fritz, J. Bhave, A. Mont, M.A. (2016). Periprosthetic joint infection. *The Lancet, 387*, 386-94

[11] Cochran, A. R., Ong, K. Ll, Lau, E., Mont, M.A., Malkani, A.L. (2016). Risk of reinfection after treatment of infected total knee arthroplasty. *The Journal of Arthroplasty, 31*, 156-161.

[12] He, X., Zhang, X., Wang, X., Qin, L. (2017). Review of Antibacterial Activity of Titanium-Based Implants' Surfaces Fabricated by Micro-Arc Oxidation. *Coatings, 7*(45).

[13] Campoccia, D., Montanaro, L, Arciola, C.R. (2013). A review of the clinical implications of anti-infective biomaterials and infection-resistant surfaces. *Biomaterials, 34*, 8018-8029.

[14] Zhao, L., Chu, P.K., Zhang, Y., Wu, Z. (2009). Antibacterial coatings on titanium implants. *Journal of Biomedical Materials Research Part B: Applied Biomaterials, 91*, 470-480.

[15] Simchi, A., Tamjid, E., Pishbin, F., Boccaccini, A.R. (2011). Recent progress in inorganic and composite coatings with bactericidal capability for orthopaedic applications. *Nanomedicine, 7*(1), 22-39.

[16] Rizwan, M., Alias, R., Zaidi, U.Z., Mahmoodian, R., Hamdi, M. (2018). Surface modification of valve metals using plasma electrolytic oxidation for antibacterial applications: A review. *Journal of Biomedical Materials Research Part A, 106*(2), 590-605.

[17] Badar, M., Rahim, M.I., Kieke, M., Ebel, T., Rohde, M., Hauser, H., Behrens, P. and Mueller, P.P. (2015). Controlled drug release from antibiotic-loaded layered double hydroxide coatings on porous titanium implants in a mouse model. *Journal of Biomedical Materials Research Part A*, *103*(6), pp.2141-2149.

[18] Hickok, N.J., Shapiro, I.M. (2012). Immobilized antibiotics to prevent orthopaedic implant infections. *Advanced Drug Delivery Review, 64*, 1165-1176.

[19] Norowski, P.A., Bumgardner, J.D. (2009). Biomaterials and antibiotic strategies for peri-implantitis. *Journal of Biomedical Materials Research Part B: Applied Biomaterials, 88*, 530–543.

[20] Campoccia, D., Montanaro, L., Arciola, C.R. (2013). A review of the biomaterials technologies for infection-resistant surfaces. *Biomaterials, 34*(34), 8533-8354

[21] Seil, J.T., Webster, T. J. (2012). Antimicrobial applications of nanotechnology: Methods and literature. *International Journal of Nanomedicine, 7*, 2767-2781.

[22] Ramyadevi, J., Jeyasubramanian, K., Marikani, A., Rajakumar, G., Rahuman, A.A. (2012). Synthesis and antimicrobial activity of copper nanoparticles. *Materials letters*, *71,* 114-116.

[23] Ruparelia, J.P., Chatterjee, A.K., Duttagupta, S.P., Mukherij, S. (2008). Strain specificity in antimicrobial activity of silver and copper nanoparticles. *Acta Biomaterialia, 4*(3), 707-716.

[24] Dizaj, S.M., Lotfipour, F., Barzegar-jalali, M., Zarrintan, M.H., Adibkia, K. (2014). Antimicrobial activity of the metals and metal oxide nanoparticles. *Materials Science & Engineering C-Materials for Biological Applications, 44*, 278-284.

[25] Li, K., Xie, Y., Huang, L., Ji, H., Zheng, X. (2013). Antibacterial mechanism of plasma sprayed Ca2ZnSi2O7 coating against Escherichia coli. *Journal of Materials Science: Materials in Medicine, 24*, 171–178.

[26] Rizzello, L., Pompa, P.P. (2014). Nanosilver-based antibacterial drugs and devices: mechanisms, methodological drawbacks, and guidelines. *Chemical Society Reviews, 43*, 1501-1518.

[27] Lemire, J.A., Harrison, J.J., Turner, R.J. (2013). Antimicrobial activity of metals: mechanisms, molecular targets and applications. *Nature Reviews, 11*, 371.

[28] Dastjerdi, R., Montazer, M. (2012). A review on the application of inorganic nano-structured materials in the modification of textiles: Focus on anti-microbial properties. *Colloids and Surfaces B: Biointerfaces, 79*, 5–18.

[29] Burghardt, I., Luthen, F., Prinz, C., Kreikemeyer, B., Zietz, C., Neumann, H.G., Rychly, J. (2015). A dual function of copper in designing regenerative implants. *Biomaterials, 44*. 36-44.

[30] Hu, H., Zhang, W., Qiao, Y., Jiang, X., Liu, X., Ding, C. (2018). Antibacterial activity and increased bone marrow stem cell functions of Zn-incorporated TiO_2 coatings on titanium. *Acta Biomaterials, 8*(2), 904-15.

[31] Hackenberg, S., Scherzed, A., Kessler, M., Hummel, S., Technau, A., Froelich, K., Kleinsasser, N. (2011). Silver nanoparticles: Evaluation of DNA damage, toxicity and functional impairment in human mesenchymal stem cells. *Toxicology Letters, 201*(1), 27–33.

[32] Bondarenko, O., Juganson, K., Ivask, A., Kasemets, K., Mortimer, M., & Kahru, A. (2013). Toxicity of Ag, CuO and ZnO nanoparticles to selected environmentally relevant test organisms and mammalian cells in vitro: a critical review. *Archives of Toxicology, 87*(7), 1181–1200.

[33] Ickrath, P., Wagner, M., Scherzad, A., Gehrke, T., Burghartz, M., Hagen, R., Hackenberg, S. (2017). Time-Dependent Toxic and Genotoxic Effects of Zinc Oxide Nanoparticles after Long-Term and Repetitive Exposure to Human Mesenchymal Stem Cells. *International Journal of Environmental Research and Public Health, 14*(12), 1590.

[34] Zhang, L., Gao, Q., Han, Y. (2016). Zn and Ag Co-doped Anti-microbial TiO_2 Coatings on Ti by Micro-arc Oxidation. *Journal of Materials Science and Technology, 32*(9), 919-924.

[35] Jin, G., Qin, H., Cao, H., Qian, S., Zhao, Y., Peng, X., Zhang, X., Liu, X., Chu, P.K. (2014). Synergistic effects of dual Zn/Ag ion implantation in osteogenic activity and antibacterial ability of titanium. *Biomaterials, 35*(27), 7699–7713.

[36] Biswas, P., Bandyopadhyaya, R. (2017). Synergistic antibacterial activity of a combination of silver and copper nanoparticle impregnated activated carbon for water disinfection. *Environmental Science: Nano, 4*(12), 2405-2417.

[37] JankauskaitĿ, V., VitkauskienĿ, A., Lazauskas, A., Baltrusaitis, J., ProsyĿevas, I., AndruleviĿius, M. (2016). Bactericidal effect of graphene oxide/Cu/Ag nanoderivatives against Escherichia coli, Pseudomonas aeruginosa, Klebsiella pneumoniae, Staphylococcus aureus and Methicillin-resistant Staphylococcus aureus. *International Journal of Pharmaceutics, 511*(1), 90–97.

[38] Moriarty, T.F., Zaat, S. A.J, Busscher, H.J. (2012). Biomaterials Associated Infection. Immunological Aspects and Antimicrobial Strategies. New York, NY: Springer.

[39] Goodman, S.B., Yao, Z., Keeney, M., Yang, F. (2013). The future of biologic coatings for orthopaedic implants. *Biomaterials, 34*, 3174-3183.

[40] Wang, J., Li, J., Guo, G., Wang, Q., Tang, J., Zhao, Y., Qin, H., Wahafu, T., Shen, H., Liu, X., Zhang, X. (2016). Silver-nanoparticles-modified biomaterial surface resistant to staphylococcus: new insight into the antimicrobial action of silver. *Scientific Reports, 6*, 32699.

[41] Head, W. C., Bauk, D. J., & Emerson Jr., R. H. (1995). Titanium as the material of choice for cementless femoral components in total hip arthroplasty. *Clinical Orthopaedics and Related Research, 311*, 85-90.

[42] Ahmadi, S.M., Yavari, S.A., Wauthle, R., Pouran, B., Schrooten, J., Weinans, H., Zadpoor, A.A. (2015). Additively manufactured open-cell porous biomaterials made from six different space-filling unit cells: the mechanical and morphological properties. *Materials, 8*, 1871-1896.

[43] Karageorgiou, V., Kaplan, D. (2005). Porosity of 3D biomaterial scaffolds and osteogenesis. *Biomaterials, 26*(27), 5474–5491.

[44] Taniguchi, N., Fujibayashi, S., Takemoto, M., Sasaki, K., Otsuki, B., Nakamura, T., Matsuda, S. (2016). Effect of pore size on bone ingrowth into porous titanium implants fabricated by additive manufacturing: An in vivo experiment. *Materials Science and Engineering: C, 59*, 690–701.

[45] Van Bael, S., Chai, Y.C., Truscello, M., Moesen, G., Kerckhofs, H., Van Oosterwyck, Kruth, J.P., Schrooten, J. (2012). The effect of pore geometry on the in vitro biological behavior of human periosteum-derived cells seeded on selective laser-melted Ti6Al4V bone scaffolds. *Acta Biomateriala, 8*, 2824-2834.

[46] Zadpoor, A.A. (2015). Bone tissue regeneration: the role of scaffold geometry, *Biomaterials Science, 3*, 231-245.

[47] Gibson, I., Rosen, D., Brent, S. (2010). Additive Manufacturing Technologies. 3D printing, Rapid Prototyping, and Direct Digital Manufacturing. Second edition. New York, United states: Springer.

[48] Popovich, A., Sufiiarov, V., Polozov, I., Borisov, E., Masaylo, D. (2016) Producing hip implants of titanium alloys by additive manufacturing. *International Journal of Bioprinting, 2*(2), 78–84.

[49] De Wild, M., Schumacher, K., Schkommodau, E., Thoma, D., Bredell, Kruse Gujer, A., Gratz, K.W., Weber, F.(2013). Bone regeneration by the osteoconductivity of porous titanium implants manufactured by selective laser melting: a histological and micro computed tomography study in the rabbit. *Tissue Engineering. Part A, 19*(23-24), 2645-2654.

[50] Castilho, M., Moseke, C., Ewald, A., Gbureck, U., Groll, J., Pires, I., Teßmar, J., Vorndran, E. (2014). Direct 3D powder printing of biphasic calcium phosphate scaffolds for substitution of complex bone defects. *Biofabrication*, 6(1):015006.

[51] Fan, H., Fu, J., Li, X., Pei, Y., Li, X., Pei, G., Guo, Z. (2015). Implantation of customized 3-D printed titanium prosthesis in limb salvage surgery: a case series and review of the literature. *World Journal of Surgical Oncology, 13*, 308.

[52] Teughels, W., Van Assche, N., Sliepen, I., Quirynen, M. (2006). Effect of material characteristics and/or surface topography on biofilm development. *Clinical Oral Implants Research, 17*(2), 68–81.

[53] Gasquères, C., Schneider, G., Nusko, R., Maier, G., Dingeldein, E., Eliezer, A. (2016). Innovative antibacterial coating by anodic spark deposition. *Surface and Coatings Technology*, *15*, 3410-3414.

[54] Marques, I.D., Barão, V.A., Da cruz, N.C., Yuan, J.C-C., Mesquiata, M.F., Ricomini-Filho, A.P., Sukotjo, C., Mathew, M.T. (2015). Electrochemical behavior of bioactive coatings on cp-Ti surface for dental application. *Corrosion Science, 100*, 133-146.

[55] Chung, C.J., Su, R.T., Chu, H.J. Chen, H.T., Tsou, H.K., He, J.L. (2013). Plasma electrolytic oxidation of titanium and improvement in osseointegration. *Journal of Biomedical Materials Research Part B, 10,* 1023-1030.

[56] Robinson, H., Markaki, A., Collier, C., Clyne, T. (2011). Cell adhesion to plasma electrolytic oxidation (PEO) titania coatings, assessed using a centrifuging technique. *Journal of the Mechanical Behavior of Biomedical Material, 4*, 2103-2112.

[57] Whiteside, P., Matykina, E., Gough, J.E., Skeldon, P., Thompson, G.E. (2010). In vitro evaluation of cell proliferation and collagen synthesis on titanium following plasma electrolytic oxidation. *Journal of Biomedical Materials Research Part A, 94*, 38-46.

[58] Necula, B.S., Van leeuwen, J.P., Fratila-apachitei, L.E., Zaat, S.A., Apachitei. I., Duszczyk, J. (2012). In vitro cytotoxicity evaluation of porous TiO_2-Ag antibacterial coatings for human fetal osteoblasts. *Acta Biomaterials*, *8*(11), 4191-7.

[59] Lu, X., Mohedano, M., Blawert, C., Matykina, E., Arrabal, R., Kainer, K.U., Zheludkevich, M.L. (2016). Plasma electrolytic oxidation coatings with particle additions – A review. *Surface and Coatings Technology, 307*, 1165-1182.

[60] Van Hengel, I.A.J., Riool, M., Fratila-apachitei, L.E., Witte-Bouma, J., Farrell, E., Zadpoor, A.A., Zaat, S.A.J., Apachitei, I. (2017). Selective laser melting porous metallic implants with immobilized silver nanoparticles kill and prevent biofilm formation by methicillin-resistant Staphylococcus aureus. *Biomaterials, 140*, 1-15.

[61] Necula, B.S., Apachitei, I., Tichelaar, F.D., Fratila-apachitei, L.E., Duszczyk, J. (2011). An electron microscopical study on the growth of TiO_2-Ag antibacterial coatings on Ti6Al7Nb biomedical alloy. *Acta Biomateriala, 7*(6), 2751-7.

[62] Putra, N.E. (2018). Antibacterial Surfaces Bearing Silver and Zinc Nanoparticles on Additively Manufactured Titanium Implants (Master thesis).

[63] Emanuel, N., Rosenfeld, Y., Cohen, O., Applbaum, Y.H., Segal, D., Barenholz, Y. (2012). A lipid-and-polymer-based novel local drug delivery system--BonyPid™: from physicochemical aspects to therapy of bacterially infected bones. *Journal of Controlled Release, 160*(2), 353-361.

[64] Gudmundsson, K. (2014). Antibacterial Surfaces to Prevent Biofilm Formation on Cementless Bone Implants (Master thesis).

[65] Valerio, V. (2018). Antibacterial silver- and copper-based surfaces on additively manufactured titanium implants (Master thesis).

[66] Necula, B.S., Van leeuwen, J.P., Fratila-apachitei, L.E., Zaat, S.A., Apachitei. I., Duszczyk, J. (2012). In vitro cytotoxicity evaluation of porous TiO_2-Ag antibacterial coatings for human fetal osteoblasts. *Acta Biomaterials*, *8*(11), 4191-4197.

[67] Hu, H., Zhang, W., Qiao, Y., Jiang, X., Liu, X., Ding, C. (2018). Antibacterial activity and increased bone marrow stem cell functions of Zn-incorporated TiO_2 coatings on titanium. *Acta Biomaterials, 8*(2), 904-15.

[68] Zhu, X.L., Chen, J., Scheideler, L., Reichl, R., Geis-Gerstorfer, J. (2004). Effects of topography and composition of titanium surface oxides on osteoblast responses. *Biomaterials, 25*, 4087–4103.

[69] Muhaffel, F., Cempura, G., Menekşe M.K., Czyrska-Filemonowicz, A., Karaguler, N., Cimenoglu, H. (2016). Characteristics of multi-layer coatings synthesized on Ti6Al4V alloy by micro-arc oxidation in silver nitrate added electrolytes. *Surface and Coatings Technology*, 307, 308-315.

[70] Broekhuizen, C.A., Schultz, M.J., Van Der Wal, A.C., Boszhard, L., De Boer, L., Vandenbroucke-Grauls, C.M., Zaat, S.A. (2008). Tissue around catheters is a niche for bacteria associated with medical device infection. *Critical Care Medicine, 36*, 2395-2402.

[71] Zaat, S.A.J., Broekhuizen, C., Riool, M. (2010). Host tissue as a niche for biomaterial- associated infection. *Future Microbiology, 5*, 1149-1151.

[72] Park, H.-J., Kim, J. Y., Kim, J., Lee, J.-H., Hahn, J.-S., Gu, M. B., & Yoon, J. (2009). Silver-ion-mediated reactive oxygen species generation affecting bactericidal activity. *Water Research, 43*(4), 1027–1032.

[73] Raghupathi, K.R., Koodali, R.T., Manna, A.C. (2011). Size-dependent bacterial growth inhibition and mechanism of antibacterial activity of zinc oxide nanoparticles. *Langmuir, 27*, 4020–4028.

[74] Sung Kim, J. Kuk, E., Yu, K.N., Kim, J-H., Park, S.J., Lee, H.J., Kim, S.H., Park, Y.H., Hwang, C-Y., Kim, Y-K., Lee, Y-S., Jeong, D.H., Cho, M-H. (2007). Experimental antimicrobial effects of silver nanoparticles. *Nanomedicine: Nanotechnology, Biology, and Medicine, 3*, 95–101

[75] Meghana, S., Kabra, P., Chakraborty, S., Padmavathy, N. (2015). Understanding the pathway of antibacterial activity of copper oxide nanoparticles. *The Royal Society of Chemistry Advances, 5*(16), 12293–12299.

[76] Morones, J.R., Elechiguerra, J.L., Camacho, A., Holt, K., Kouri, J.B., Ramirez, J.T, Yacaman, M.J. (2005). The bactericidal effect of silver nanoparticles. *Nanotechnology, 16*, 2346–53.

[77] Sondi, I., Sondi, B. S. (2004). Silver nanoparticles as antimicrobial agent: A case study on E. coli as a model for gram-negative bacteria. *Journal of Colloid and Interface Science, 275*, 177.

[78] Del Curto, B., Brunella, M. F., Giordano, C., Pedeferri, M. P., Valtulina, V., Visai, L., & Cigada, A. (2005). Decreased Bacterial Adhesion to Surface-Treated Titanium. *The International Journal of Artificial Organs, 28*(7), 718–730.

[79] Taner, M., Sayar, N., Yulug, I. G., & Suzer, S. (2011). Synthesis, characterization and antibacterial investigation of silver–copper nanoalloys. *Journal of Materials Chemistry, 21*(35), 13150.

[80] Jin, G., Qin, H., Cao, H., Qian, S., Zhao, Y., Peng, X., Chu, P. K. (2014). Synergistic effects of dual Zn/Ag ion implantation in osteogenic activity and antibacterial ability of titanium. *Biomaterials, 35*(27), 7699–7713.

[81] Jin, G., Qin, H., Cao, H., Qiao, Y., Zhao, Y., Peng, X., … Chu, P. K. (2015). Zn/Ag micro-galvanic couples formed on titanium and osseointegration effects in the presence of S. aureus. *Biomaterials, 65*, 22–31.

[82] Zhang, L., Guo, J., Yan, T., Han, Y. (2018). Fibroblast responses and antibacterial activity of Cu and Zn co-doped TiO_2 for percutaneous implants. *Applied Surface Science*, *434,* 633-642.

[83] Zhang, L., Guo, J., Huang, X., Zhang, Y., Han, Y. (2016). The dual function of Cu-doped TiO_2 coatings on titanium for application in percutaneous implants. *Journal of Materials Chemistry B, 4*, 3788–3800.

[84] Zhang, L., Gao, Q., Han, Y. (2016). Zn and Ag Co-doped Anti-microbial TiO_2 Coatings on Ti by Micro-arc Oxidation. *Journal of Materials Science & Technology, 32*(9), 919-924

[85] Lan, Z., Guo-Hua, L., Fei-Fei, M., Si-Ze, Y. (2014).Preparation of biomedical Ag incorporated hydroxyapatite/titania coatings on Ti6Al4V alloy by plasma electrolytic oxidation. *Chinese Physics B, 23*(3); DOI: 10.1088/1674-1056/23/3/035205

[86] Necula, B.S. (2013). Silver-based antibacterial surfaces for bone implants, in Biomaterials and Tissue Biomechanics (Dissertation).

[87] Zhao, D., Lu, Y., Zeng, X., Wang, Z., Liu, S., Wang, T. (2017). Antifouling property of micro-arc oxidation coating incorporating Cu_2O nanoparticles on Ti6Al4V. *Surface Engineering, 33(10),* 796-802

[88] Roknian, M., Fattah-Alhosseini, A., Gashti, O.S., Keshavarz, M.K. (2018). Study of the effect of ZnO nanoparticles addition to PEO coatings on pure titanium substrate: Microstructural analysis, antibacterial effect and corrosion behavior of coatings in Ringer's physiological solution. *Journal of Alloys and Compounds, 740*, 330-345.

[89] Romanò, C.L., Scarponi, S., Gallazzi, E., Romanò, D., Drago, L. (2015) Antibacterial coating of implants in orthopaedics and trauma: a classification proposal in an evolving panorama. *Journal of Orthopaedic Surgergy and Research, 10*, 157.

[90] Anderson, J. M. (1993). Chapter 4 Mechanisms of inflammation and infection with implanted devices. *Cardiovascular Pathology, 2*(3), 33–41.

[91] Tierolf, M.W.A.M. (2018). Antibacterial ability of titanium surfaces containing antibacterial metal elements fabricated by plasma electrolytic oxidation: A Systematic Review (Literature Review).

[92] Campoccia, D., Montanaro, L., & Arciola, C. R. (2006). The significance of infection related to orthopedic devices and issues of antibiotic resistance. *Biomaterials, 27(*11), 2331–2339.

[93] Katsikogianni, M., Missirlis, Y.F. (2004). Concise review of mechanisms of bacterial adhesion to biomaterials and of techniques used in estimating bacteria-material interactions. *European Cells and Materials Journal, 8,* 37–57.

[94] Trampuz, A., & Widmer, A. F. (2006). Infections associated with orthopedic implants. *Current Opinion in Infectious Diseases, 19*(4), 349–356.

[95] Cheng, H., Li, Y., Huo, K., Gao, B., & Xiong, W. (2013). Long-lastingin vivo and in vitro antibacterial ability of nanostructured titania coating incorporated with silver nanoparticles. *Journal of Biomedical Materials Research Part A, 102*(10), 3488–3499.

[96] Yao, X., Zhang, X., Wu, H., Tian, L., Ma, Y., & Tang, B. (2014). Microstructure and antibacterial properties of Cu-doped TiO_2 coating on titanium by micro-arc oxidation. *Applied Surface Science, 292*, 944–947.

[97] Yamamoto, A., Honma, R., & Sumita, M. (1998). Cytotoxicity evaluation of 43 metal salts using murine fibroblasts and osteoblastic cells. *Journal of Biomedical Materials Research, 39*(2), 331–340.

[98] Zhang, W., Jiang, P., Chen, W., Zheng, B., Mao, Z., Antipov, A., … Gao, C. (2016). Genotoxicity of Copper Oxide Nanoparticles with Different Surface Chemistry on Rat Bone Marrow Mesenchymal Stem Cells. *Journal of Nanoscience and Nanotechnology, 16*(6), 5489–5497.

[99] Albers, E., Hofstetter, W., Siebenrock, K.A., Landmann, R., Klenke, F.M. (2013). In vitro cytotoxicity of silver nanoparticles on osteoblasts and osteoclasts at antibacterial concentrations. *Nanotoxicology, 7*, 30-36.

[100] Park, T.E., Choe, H.C., Brantley, W.A. (2013). Bioactivity evaluation of porous TiO_2 surface formed on titanium in mixed electrolyte by spark anodization. *Surface and Coatings Technology, 235,* 706–713.

[101] Sul, Y. (2003). The significance of the surface properties of oxidized titanium to the bone response: special emphasis on potential biochemical bonding of oxidized titanium implant. *Biomaterials, 24(*22), 3893–3907.

[102] Zhu, W., Zhang, Z., Gu, B., Sun, J., Zhu, L. (2013). Biological activity and antibacterial property of nano-structured TiO_2 coating incorporated with Cu prepared by micro-arc oxidation. *Journal of Materials Science & Technology, 29*, 237–244

[103] Goers, L., Freemont, P., & Polizzi, K. M. (2014). Co-culture systems and technologies: taking synthetic biology to the next level. *Journal of The Royal Society Interface, 11*(96), 20140065–20140065.

[104] McConda, D. B., Karnes, J. M., Hamza, T., & Lindsey, B. A. (2016). A novel co-culture model of murine K12 osteosarcoma cells and *S. aureus* on common orthopedic implant materials: "the race to the surface" studied in vitro. *Biofouling, 32*(6), 627–634.

9 Appendices

9.1 Macroscopic analysis of the implants

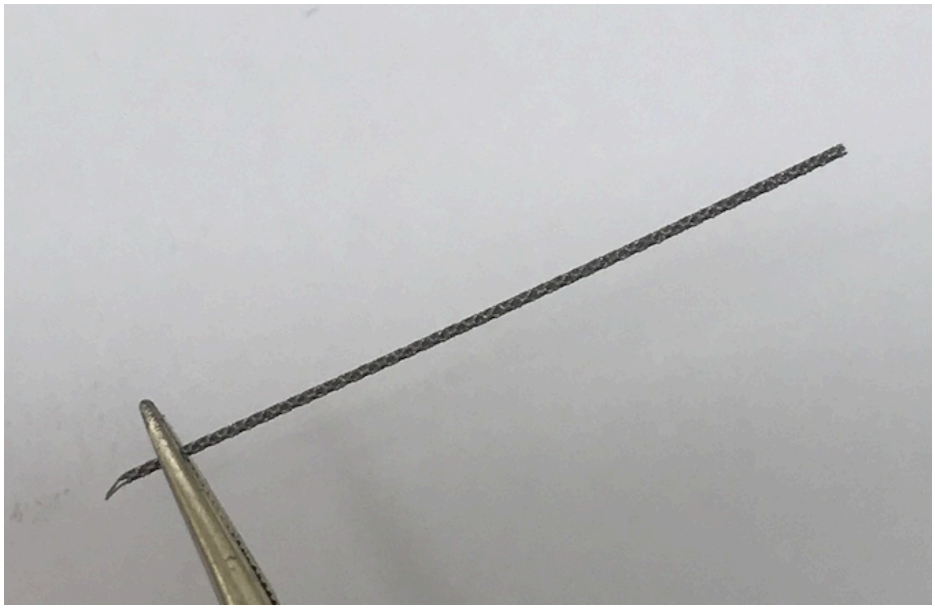

Fig. 19. Medical grade Ti6Al4V implants as manufactured by SLM.

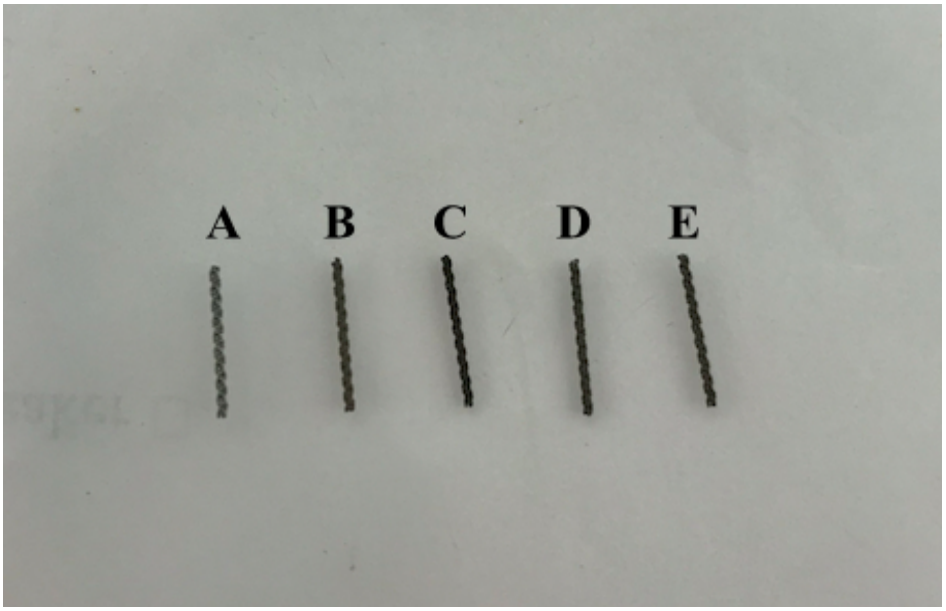

Fig. 20. Set of SLM Ti6Al4 implants. (A) Prior to PEO processing, NT. (B) PEO processing without NPs, PT. (C) PEO processing with Ag NPs. (D) PEO processing with Cu NPs. (E) PEO processing with Zn NPs.

9.2 Release kinetics of the ions

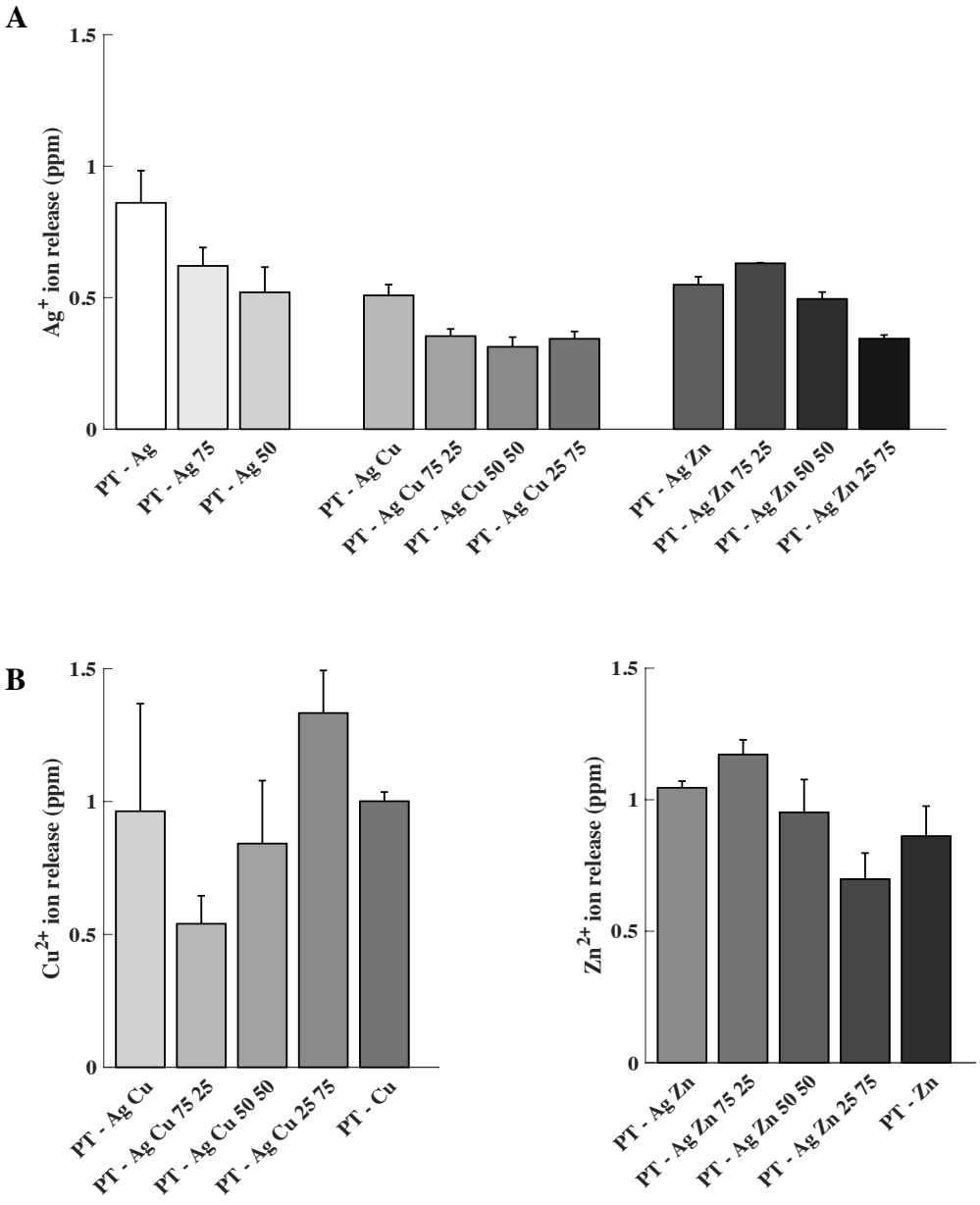

Fig. 21. Cumulative release of the (A) Ag^{+} ions, (B) Cu^{2+} ions and (C) Zn^{2+} ions from the implants with NPs, within 24 h.

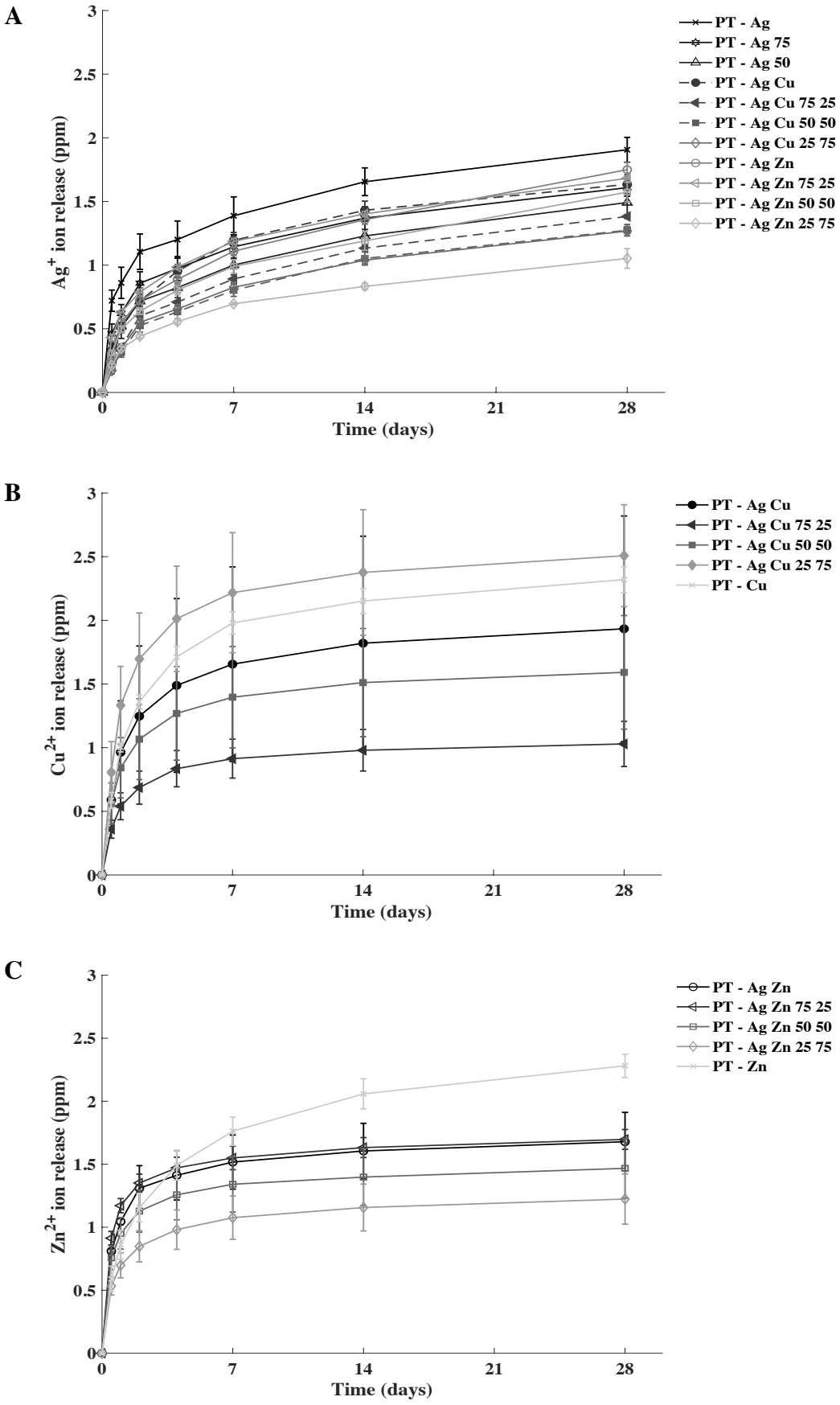

Fig. 22. Cumulative release kinetics of the (A) Ag^{+} ions, (B) Cu^{2+} ions and (C) Zn^{2+} ions from the implants with NPs, up to 28 days.